



Tectono-metamorphic interaction of upper mantle peridotites and lower crustal units during continental rifting in the western Betic Cordillera

Juan Díaz-Alvarado^{a,*}, Luis González-Menéndez^b, Károly Hidas^b, Antonio Azor^c, Antonio Pedrera^b

^aDepartamento de Biología y Geología, Física y Química Inorgánica, ESCET, Universidad Rey Juan Carlos, Av. del Alcalde de Móstoles, 28933 Móstoles, Spain

^bInstituto Geológico y Minero de España (IGME), CSIC, Calle de Ríos Rosas 23, 28003 Madrid, Spain

^cDepartamento de Geodinámica, Universidad de Granada, Avenida de la Fuente Nueva s/n, 18071 Granada, Spain

ARTICLE INFO

Article history:

Received 31 January 2024

Revised 27 March 2024

Accepted 31 March 2024

Available online 9 May 2024

Handling Editor: Jan Marten Huizenga

Keywords:

Continental rifting
Lower-crust migmatite
Mantle peridotite
Guadaiza unit
Ronda massif
Betic Cordillera

ABSTRACT

Recent geological mapping conducted in the Ronda Peridotites (Betic Cordillera, S Spain) has revealed a systematic field correlation between lower crustal metamorphic units and different tectono-metamorphic domains of the ultramafic massif. Mylonitic and highly tectonized Spl ± Grt peridotites (i.e., Grt-Spl mylonite and Spl tectonite domains), which are considered to be derived from a thick continental lithosphere, are in contact with garnet-bearing gneisses (i.e., kinzigites) of the Jubrique unit along a narrow but continuous mylonitic shear zone. Phase equilibrium calculations indicate that the metamorphic rocks of the Jubrique unit are consistent with an initial continental setting characterized by normal crustal thicknesses, which underwent two melting events. The first melting occurred at 0.9–1.0 GPa / 770–800 °C and resulted in 13 % melt, while the second one took place at shallower crustal conditions (0.4–0.5 GPa and 710–765 °C) and led to more restricted melt production (2–3 % melt). In contrast, the Spl ± Pl peridotites (Pl-tectonite domain), which are stable only at shallowest mantle levels within a highly extended continental lithosphere, are consistently found exposed in contact with heterogeneous granites and migmatites of the Guadaiza unit. According to new thermodynamic modeling, the Guadaiza metamorphic rocks record a single melting event characterized by a theoretical melt production of 6 to 11 % at the base of a very thin continental crust (ca. 0.3 GPa and 675–710 °C). This process was likely facilitated by influx of external water, necessary to generate high melt fractions observed in the diatexites. The systematic correlation observed between crustal metamorphic units, consistently overlaying the mantle rocks, and specific ultramafic domains of the Ronda massif, suggests that their juxtaposition primarily resulted from the severe extension of the continental lithosphere.

U-Pb radiometric dating of zircons from gneisses, migmatites, and heterogeneous granites in the middle crustal rocks of the Guadaiza unit indicates that extensional processes, crustal anatexis, and melt stagnation occurred at around 280 Ma. Comparison of these new radiometric ages with previous results from the Jubrique unit suggests that a Permian high-temperature / low- to medium-pressure event uniformly affected the crustal units over the Ronda Peridotites. This event coincided with the formation of characteristic ultramafic mineral assemblages within the Ronda massif and provides evidence for the interaction between upper mantle rocks and lower- to mid-crustal metamorphic rocks during this period.

© 2024 The Author(s). Published by Elsevier B.V. on behalf of International Association for Gondwana Research. This is an open access article under the CC BY license (<http://creativecommons.org/licenses/by/4.0/>).

1. Introduction

Continental rifts represent emerging plate boundaries where ongoing tectonic activity progressively thins the lithosphere and, eventually, leads to the break-up and splitting of the continental landmass (e.g., Brune et al., 2023). This tectonic evolution is often observed in mid- to lower crustal metamorphic rocks and underly-

ing ultramafic rocks of the upper mantle, which record the substantial pressure and temperature changes through the formation of new mineral parageneses, driven by a series of re-equilibration processes (e.g., Soto and Platt, 1999; Müntener et al., 2000). As the rift matures, a combination of preexisting internal weaknesses and newly forming extensional structures in the lithosphere contribute to crustal thinning and upper mantle uplift (e.g., Theunissen and Huisman, 2022; Brune et al., 2023 and references therein). In the final stages of lithosphere thinning – usually referred to as hyperextension of the continental lithosphere –, this

* Corresponding author.

E-mail address: juan.diaza@uda.cl (J. Díaz-Alvarado).

process may result in the exposure of the upper mantle at surface across the transition zone between continental and oceanic crust (e.g., Pérez-Gussinyé, 2013), as reported from various rifted margins worldwide (e.g., Whitmarsh et al., 2001; Manatschal, 2004; Sawyer et al., 2007; Mohn et al., 2014).

Tectonic inheritance and melt-weakening processes are known to be key factors in the development of rifts (Díaz-Alvarado et al., 2021; Corti et al., 2022; Zheng et al., 2022). In these settings, granite-migmatite-granulite associations are typically produced by crustal anatexis (Zheng and Chen, 2021; Zheng and Gao, 2021). Continental rifts typically originate within former orogenic belts, and conversely, new orogens often form over previously rifted regions (e.g., Vauchez et al., 1997; Peron-Pinvidic and Osmundsen, 2020; Zheng and Gao, 2021; Peron-Pinvidic et al., 2022). In both cases, characterizing early deformation events can be particularly challenging because subsequent deformations, metamorphic and/or magmatic processes can potentially erase or disrupt the original paragenetic and geochronological data. Seismic reflection profiles of the present-day ocean margins provide information on the deformation style and allow discussing the mechanisms promoting continental rifting (e.g., Clerc et al., 2018; Peron-Pinvidic et al., 2019). However, geophysical data alone cannot constrain the age and composition of the lithosphere, nor the thermal conditions during deformation. Therefore, understanding the processes that control the rheological evolution are usually addressed by thermomechanical modeling (e.g., Huisman and Beaumont, 2011, 2014; Brune et al., 2014). On the other hand, in recent years hyperextended domains preserved within certain collisional orogens, such as the Pyrenees and Alps have been widely recognized (e.g., Jammes et al., 2009; Lagabrielle et al., 2010; Tugend et al., 2014; Manatschal et al., 2015; Pedrera et al., 2017, 2021, 2023; Gómez-Romeu et al., 2019). Studying these regions provides a unique opportunity to analyze melt-rock reactions in the lower crust and uppermost mantle during continental rifting. It also offers insight into the relation between ductile deformation processes and normal faulting, while aiding in constraining the timing of extensional processes. Nevertheless, due to the long and complex tectonic and magmatic history of continental rifts, absolute dating of the different stages of their evolution is still a challenging task.

The Ronda Peridotites, widely exposed in the inner zone of the Betic Cordillera, are the result of drastic lithosphere-scale attenuation processes (e.g., Garrido et al., 2011; Obata, 1980; Platt et al., 2003a; Prêçigout et al., 2013; Van der Wal and Bodinier, 1996; Van der Wal and Vissers, 1993; Van Der Wal and Vissers, 1996; Bessièrre et al., 2021; Sánchez-Gómez et al., 2002), during which the crustal envelope of the mantle rocks underwent partial melting (e.g., Lundeen, 1978; Balanyá et al., 1997; Tubía et al., 1997; Argles et al., 1999; Platt et al., 2003a; Esteban et al., 2008; Acosta-Vigil et al., 2014). The age of this partial melting and the role played by the peridotites have been extensively debated, resulting in contrasting and contradictory proposals (Acosta-Vigil et al., 2014; Argles et al., 1999; Balanyá et al., 1997; Garrido et al., 2011; Platt et al., 2003a,b; Ruiz Cruz and Sanz de Galdeano, 2014; Sosson et al., 1998; Tubía et al., 1997). This controversy partly stems from the fact that in the most robust U-Th-Pb zircon geochronology, zircons that have undergone dissolution, recrystallization, or have been affected by alteration or metamorphism are prone to resetting or changes in their isotope composition (e.g., Pb loss) during the prolonged evolution of continental rifts.

In this study, we present a new geological map of the Ronda Peridotites, as well as thermodynamic modeling, geochemistry, and radiometric dating of the Guadaiza metamorphic unit that overlies the plagioclase-tectonite domain of the ultramafic body. These new data allow for establishing the spatial relationship and the mutual metamorphic evolution between the crustal units

and the different domains of the peridotites. Therefore, we explore the deformation style and tectono-metamorphic evolution in both the upper mantle peridotites and the overlying lower crustal units. The aim of the geochronological study is to unravel the coincidence of Late Paleozoic and younger, up to Early Miocene, ages in samples from the Western Betic Cordillera based on recrystallization ages of zircons in migmatitic and metamorphic crustal units around the Ronda Peridotites. Our results provide information on the feedback between crustal melting and uppermost mantle re-equilibration during continental rifting.

2. Geological background

2.1. Geology of the Betic Cordillera

The Betic Cordillera in southern Spain and the Rif Mountains in northern Morocco constitute an Alpine collisional orogen located at the present-day convergent boundary of the Iberian and African plates (Fig. 1). The pre-orogenic evolution of the Betic Cordillera includes two overlapping continental rifting cycles of Permian-Triassic and Jurassic-Early Cretaceous age (e.g., Vera et al., 2004; Jabaloy-Sánchez et al., 2019) which culminated in the formation of oceanic crust and the development of hyperextended passive margins with exhumed mantle domains between the two major plates (e.g., Pedrera et al., 2021). The orogenic evolution resulted from the subduction of the intervening oceanic domains and oblique collision of the continental paleo-margins of southern Iberia and northern Africa (Blanco and Spakman, 1993; Morley, 1993; Royden, 1993; Lonergan and White, 1997; Gill et al., 2004; Thiebot and Gutscher, 2006; Pedrera et al., 2011, 2020; Ruiz-Constán et al., 2011).

Three major geological units are recognized in the Betic Cordillera (Vera et al., 2004): a) the External Zones, made up of Mesozoic and Cenozoic sedimentary rocks, generally interpreted as the detached overburden of the South Iberian margin; b) the Campo de Gibraltar Complex, restricted to the western part of the orogen and composed of Cretaceous and Tertiary turbiditic sequences; and c) the Internal Zones, made up of Paleozoic and Mesozoic rocks, which are organized in variably thinned units recording ductile deformation and metamorphism (e.g., Fallot, 1948; Jabaloy-Sánchez et al., 2019) (Fig. 1).

The Internal Zones are usually subdivided into three major tectono-metamorphic units, which are, from top to bottom: the Maláguide Complex, the Alpujárride Complex and the Nevado-Filábride Complex, the latter being restricted to the central and eastern part of the mountain range. It is classically assumed that these units are tectonically stacked and that they represent different paleogeographic domains. Overall, the Internal Zones are generally interpreted as a microplate, the so-called Alborán Domain, which collided with the Iberian and African paleomargins (Andrieux et al., 1971; Bouillin et al., 1986; Balanyá and García Dueñas, 1987, 1991). However, the evolution and palaeogeographical assignment of these tectono-metamorphic units, as well as the amount of displacement and the trajectory of the Alborán Domain during the collision are subject to debate (e.g., Vergés and Fernández, 2012; Casciello et al., 2015; Pedrera et al., 2020).

The Maláguide complex is situated at the uppermost structural position and consists of a Paleozoic basement only affected by low- to very low-grade Variscan metamorphism, overlain by an unmetamorphosed Mesozoic to Cenozoic cover (e.g., Cuevas et al., 2001; Martín-Algarra et al., 2009). Below the Maláguide, the Alpujárride complex recorded a pre-Alpine and Alpine tectonometamorphic evolution associated with two distinct geodynamic processes (e.g., Acosta-Vigil et al., 2014; Massonne, 2014; Sánchez-Navas et al., 2017). The prevailing interpretation

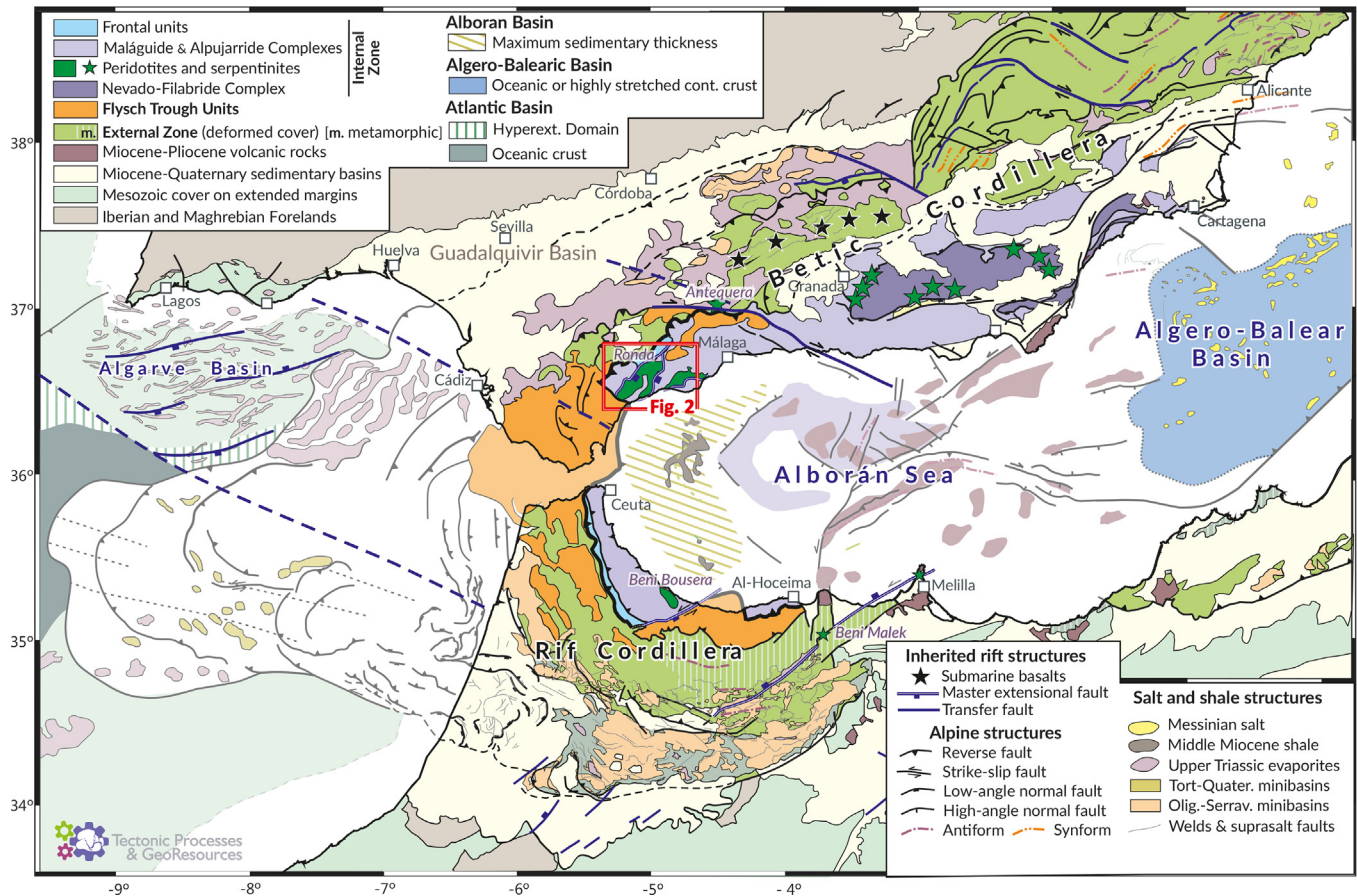


Fig. 1. Simplified tectonic map of the Betic-Rif Cordillera and adjacent continental and oceanic margins indicating the inherited Mesozoic rift structures (modified from Pedrera et al., 2020). The location of the geological map of the Fig. 2 is indicated.

suggests that the Alpujarride complex comprises several overlapping tectonic units, which are highly attenuated, with the structurally upper units located in the western part of the orogen and the lower ones exposed in the central and eastern part of the Betics, overlying the Nevado-Filábride complex (Fig. 1). The lower part of the Alpujarride sequence in the western Betics consists of lithospheric mantle peridotites overlaid by gneisses and migmatites, which are widely exposed in the study area (Figs. 1 and 2). Above these lithologies, there are dark- and light-colored schists and quartz-schists of Paleozoic age. On top of the schists, phyllites and quartzites assigned to the Permo-Triassic are found, followed by limestones and dolostones that exhibit variable degrees of recrystallization to marbles, attributed to the Triassic (e.g. Balanyá et al., 1997). Despite the wealth of available geological data, the tectono-metamorphic evolution of the western Alpujarride units remains controversial, particularly concerning their relationship with the mantle domains, the timing of crustal partial melting and peridotite emplacement, as well as the large-scale geodynamic processes involved.

2.2. Ronda Peridotites

Subcontinental mantle peridotites, known as the Ronda Peridotites, extensively crop out in the western part of the Betic Cordillera as isolated ultramafic bodies, ranging in size from < 1 km² completely serpentinized exposures to the 300 km² Ronda massif (Sierra Bermeja), covering altogether approximately 450 km² (Figs. 1 and 2). Lherzolite and harzburgite with minor dunitic lithologies dominate the exposure, whereas different types of

mafic pyroxenite layers usually represent < 5 % (Garrido and Bodinier, 1999). The western transect of the Ronda massif, which concentrates the majority of studies, is divided from northwest to southeast into four, km-scale lithological domains referred to as (i) Grt-Spl mylonites, (ii) Spl tectonites, (iii) granular Spl peridotites and (iv) Pl tectonites (Fig. 2; Obata, 1980; Van der Wal and Vissers, 1996), each one exhibiting distinctive structures and metamorphic assemblages formed during the exhumation of the mantle sequence (e.g., Garrido et al., 2011 and references therein). However, eastwards not all of these domains are present, and the Pl-bearing peridotites dominate the ultramafic exposures (Obata, 1980; Fig. 2) (mineral abbreviations by Whitney and Evans, 2010).

The Grt-Spl mylonites are interpreted either as younger structures formed during high-P shearing of the Spl tectonites (e.g., Van der Wal and Vissers, 1996), or coeval to them and indicating an increasing strain localization towards the contact with the crustal metamorphic units (Précigout et al., 2007; Garrido et al., 2011; Précigout et al., 2013). Alternative models suggest that the Grt-Spl mylonites are the result of subduction of previously exhumed Spl lherzolite facies peridotites back to the Grt stability field (Van der Wal and Vissers, 1993), or propose that the mylonitization of Grt peridotites occurred at rather low pressures in the Spl lherzolite facies (1.2–0.8 GPa at 850–900 °C; Johannesen et al., 2014). Overall, the Grt-Spl mylonite and Spl tectonite domains are more consistent with decompression, cooling and strain localization from approximately 1100 °C and 2.7 GPa (as recorded in remnants of Grt peridotites in the Grt-Spl mylonite domain) to 800–900 °C at < 2 GPa (Précigout et al., 2007; Garrido et al., 2011; Johannesen et al., 2014) during extensional deformation of the continental

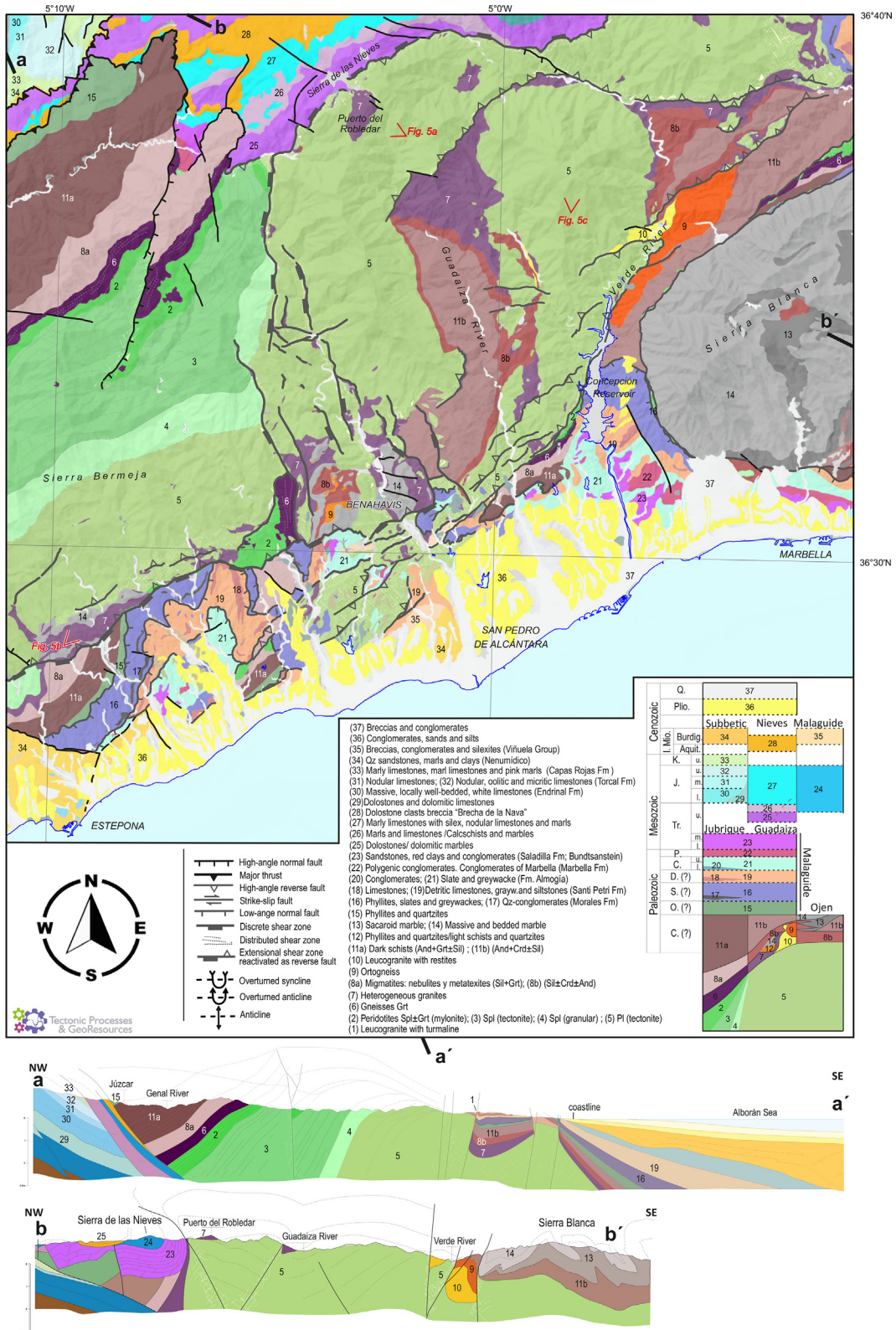


Fig. 2. Geological map and selected cross-sections of the studied area.

lithosphere (Platt et al., 2003a, 2013). This significant thinning is also supported by the existence of graphite pseudomorphs after diamond in some Grt pyroxenites (Davies et al., 1993).

In the western part of the Ronda massif, the Spl tectonite domain is replaced by granular Spl peridotites across a sharp yet

continuous contact, referred to as recrystallization or coarsening front, which is interpreted as a thermal boundary layer above partially molten Spl tectonite protoliths (Van der Wal and Bodinier, 1996; Lenoir et al., 2001; Soustelle et al., 2009). The granular Spl peridotites record temperatures > 1200 °C at 1.5 GPa (Lenoir

et al., 2001) and preserve crystallographic preferred orientation (CPO) inherited from earlier tectonic events that deformed the Spl tectonite domain (Vauchez and Garrido, 2001). Alternatively, the partial melting recorded in the granular Spl peridotites preceded the deformation event that formed the Spl tectonite domain, and the Spl tectonites formed in distributed shear zones overprinting part of the granular Spl peridotites (Johanesen et al., 2014). The granular Spl peridotites pass into porphyroclastic Pl tectonites (Obata, 1980; Van der Wal and Vissers, 1996; Hidas et al., 2013a). This phase transformation records late low-P cooling of the mantle section at 800–900 °C and 0.5–0.7 GPa (Obata, 1980), which is also attested by the retrograde breakdown of Grt in Grt pyroxenites of the older tectonometamorphic domains, where kelyphite coronas formed at 620–700 °C and 0.4–0.8 GPa (Obata, 1994). The foliation of the Pl tectonite domain is interpreted either as a result of localized deformation in km-scale shear zones (Van der Wal and Vissers, 1993, 1996), or as the axial plane of a km-scale fold (Hidas et al., 2013a). Independently of the invoked structural interpretation, this fabric is related to the emplacement of the ultramafic rocks in the crust. The final stages of deformation, associated with the crustal emplacement of the massif, led to ductile strain localization within pyroxenite and peridotite shear zones ranging from centimeter to several decameters in thickness (Hidas et al., 2013b; 2016). The strain localization was probably accompanied by synkinematic fluid circulation in the shear zones (Hidas et al., 2016; Précigout et al., 2017), occurred at < 0.8 GPa and < 800 °C (Hidas et al., 2013b, 2016).

2.3. Crustal units

Three tectono-metamorphic units are distinguished within the western Alpujárride Complex, namely the Jubrique, Guadaiza, and Ojén units (Navarro-Vilá and Tubía, 1983; Tubía, 1985; Martín-Algarra and Vera, 2004). Below, we present the Jubrique and Guadaiza units, which are exposed in the study area (Fig. 2).

The Grt-Spl mylonite domain of the Ronda Peridotites is covered by the Jubrique crustal sequence, which underwent partial melting close to its contact with the peridotites (Lundeen, 1978; Balanyá et al., 1997; Tubía et al., 1997; Argles et al., 1999; Acosta-Vigil et al., 2001; Platt et al., 2003a; Esteban et al., 2008). At the contact, the crustal rocks are Grt-bearing blastomylonitic gneisses and migmatites (Loomis, 1972; Balanyá et al., 1997; Platt et al., 2003a; Barich et al., 2014). Far away from the contact with the peridotites, the Jubrique unit is overlaid by essentially unmetamorphosed Paleozoic rocks of the Maláguide Complex (e.g., Hoepfner et al., 1963, 1964; Tubía, 1988; Balanyá and García-Dueñas, 1991; Tubía et al., 1993; Balanyá et al., 1997).

The metamorphic conditions range from 1.3 to 1.4 GPa and 700–800 °C at the bottom of the Jubrique sequence, in contact with the ultramafic rocks, through amphibolite- and greenschist facies rocks in the middle part, to carbonates and phyllites at the top, which recorded HP-LT conditions (0.7–0.8 GPa and < 450 °C) (Torres-Roldán, 1981; Azañón et al., 1995; Balanyá et al., 1997; Platt et al., 2003a).

Melting in Jubrique-type rocks has been related to decompression during crustal thinning (Argles et al., 1999; Platt et al., 2003a). Barich et al. (2014), Massonne (2014) and Acosta-Vigil et al. (2016) calculated P-T pseudosections for the Jubrique gneisses and defined two P-T domains where melting took place. A high-pressure early melting (1.15–1.40 GPa and 740–850 °C) was established based on Grt major element zoning and Ky-Rt inclusions. According to Barich et al. (2014) and Acosta-Vigil et al. (2016), a second melting process took place at lower pressures (0.45–0.58 GPa and 775–845 °C), characterized by Grt with Sil-Ilm inclusions and Crd + Bt + Qz rims. Granite nano-inclusions within Grt were described for both melting events.

Similar to the Jubrique unit, the metamorphic rocks assigned to the Guadaiza unit show a high thermal gradient from basal migmatites and nebulitic migmatites (the so-called heterogeneous granites) to low-grade metasediments dominated by dark schists intercalated with quartzites, phyllites, and massive marbles (Tubía, 1988; Balanyá and García-Dueñas, 1991; Sanz de Galdeano, 2017, 2023). Most authors interpret that the Guadaiza unit is overthrust by the Ronda Peridotites, thus, one of the key exposures of the unit in the Guadaiza river valley has been generally considered as a tectonic window (e.g., Balanyá and García-Dueñas, 1991; Lundeen, 1978; Muñoz, 1991; Sánchez-Gómez et al., 1995, 2002; Tubía, 1988; Tubía and Cuevas, 1986; Martín-Algarra and Vera, 2004; Esteban et al., 2008; Platt et al., 2013; Précigout et al., 2013). According to those authors, the Ronda Peridotites would overlie a “migmatitic breccia” along the contact, which would have been formed as a dynamothermal aureole during Alpine thrusting and shearing (e.g., Lundeen, 1978; Torres-Roldán, 1983; Tubía and Cuevas, 1986; Tubía et al., 1997, 2013; Esteban et al., 2008). Nevertheless, early field studies proposed that the Guadaiza metamorphic crustal sequence overlies the ultramafic rocks (e.g., Loomis, 1972, 1975; Chamón-Cobos et al., 1978; Piles Mateo et al., 1978; Torres-Roldán, 1983), a view that has been endorsed in some recent works (Sanz de Galdeano and Ruiz Cruz, 2016; Sanz de Galdeano, 2017, 2023, and references therein).

In the schists and migmatitic metasedimentary rocks of the Guadaiza unit, as well as in the migmatitic orthogneisses exposed close to Istán, the metamorphic assemblages include Crd, And, and occasionally Sil, which have been interpreted as indicative of HT-LP conditions (Esteban et al., 2008; Acosta-Vigil et al., 2014). The main migmatization event recorded by the Istán migmatites occurred at 675–750 °C and 0.30–0.35 GPa (Acosta-Vigil et al., 2014).

Leucogranite dykes, mostly intruded along serpentinized brittle faults in the Ronda peridotites, crosscut the main foliation of the Jubrique and Guadaiza metasedimentary sequences (Cuevas et al., 2006; Esteban et al., 2008). These leucogranites have been dated at 20–22 Ma (U-Pb on zircons) (Sánchez-Rodríguez, 1998; Sánchez-Rodríguez and Gebauer, 2000; Esteban et al., 2007, 2011a).

2.4. Geochronological results recording partial melting in the studied mantle and crustal sequence

Numerous studies in the area have attributed high-grade metamorphism and partial melting in the migmatitic rocks at the base of the crustal units to either Variscan (Rif mountains: Michard et al., 1997; Bouybaouene et al., 1998; Montel et al., 2000; Rossetti et al., 2010; Betic cordillera: Acosta-Vigil, 1998; Sánchez-Rodríguez, 1998; Gómez-Pugnaire et al., 2004; Acosta-Vigil et al., 2014; Sanz de Galdeano and López Garrido, 2016; Sanz de Galdeano, 2017) or Alpine processes (Rif mountains: Rossetti et al., 2010; Betic cordillera: Loomis, 1975; Sánchez-Rodríguez and Gebauer, 2000; Whitehouse and Platt, 2003; Esteban et al., 2011a). Recently, Sánchez-Navas et al. (2024) have defined two clockwise metamorphic stages in metapelites and orthogneisses of the Upper Alpujárride unit: a pre-Alpine latest Carboniferous to Permian event and the metamorphism associated with the Alpine orogenic cycle (Miocene).

Regarding mantle rocks, although the sequence of development of the different tectono-metamorphic domains is relatively well constrained, absolute age data from the Ronda Peridotites is scarce. Nevertheless, Sánchez-Rodríguez and Gebauer (2000) reported Late Carboniferous to Early Permian (285, 282 ± 11 and 260 ± 11 Ma), Toarcian (178 ± 3 Ma) and Early Cretaceous (131 ± 3 Ma) ages in magmatic zircons from the high-P Grt pyroxenites of the Grt-Spl mylonite domain. These authors interpreted that the pyroxenites formed at Late Jurassic–Early Cretaceous

times, while older ages would be inherited. In addition, Lu-Hf dating in Grt yielded Jurassic-Early Cretaceous (144 ± 2), Eocene (53 ± 2 Ma) and Miocene (21 ± 30 Ma) ages (Barich, 2015), although the youngest one is admittedly uncertain.

Chromitite bodies, exposed near the contact with Guadaiza-type crustal rocks near Estepona, show a foliation parallel to the fabric of the Pl tectonite, interpreted as high-temperature deformation during magmatic crystallization (González-Jiménez et al., 2017). Concordant Early Jurassic (192 ± 13 Ma) and Cretaceous (109 ± 15 Ma) ages were obtained from the core and rim, respectively, of a single zircon from these chromitites (González-Jiménez et al., 2017).

Amphibolite with eclogite assemblage relict from the Ojén Unit is consistent with the characteristics of basaltic magmas that are derived from partial melting of either an enriched or transitional state mantle source (Tubía et al., 2009). U-Pb-Th ages from magmatic oscillatory-zoned domains in zircons give 180–185 Ma ages (Sánchez-Rodríguez and Gebauer, 2000).

3. New structural data: Field relationships between peridotites and crustal rocks

We carried out new, detailed geological mapping and associated geological cross sections with specific focus on the eastern section of the Ronda massif and its crustal surroundings, which encompasses the Alpujárride and Maláguide complexes. Our study area extends from the N-NW of Marbella to the S-SE of Ronda (Figs. 1 and 2).

3.1. The Jubrique unit and associated ultramafic rocks

In the western part of the study area, the best exposed section of the Jubrique unit consists of a sequence of metamorphic rocks that overlie the Ronda Peridotites. The metamorphic grade increases progressively towards the lower part of the crustal sequence. Small outcrops of the same crustal-mantle sequence are also found west of Montemayor, northeast of San Pedro de Alcántara, south of Sierra Alpujata, and along the northern edge of Sierra Blanca (Fig. 2). The entire crustal section reaches a maximum thickness of 5 km (≈ 9 km including the overlying Maláguide complex) and has a constant dip of 40–50° to the northwest. The petrologic Moho is characterized by a several-meter thick mylonitic shear zone, which marks the boundary between the base of the crustal section (Grt-gneisses) and the top of the ultramafic pile (mylonitic Spl \pm Grt peridotites) (Figs. 2, 3). Consequently, the foliation observed in both the crustal and mantle rocks is nearly parallel to this broad shear zone, becoming more pronounced and intense towards the Moho, where strain reaches its maximum. In the northern part of the study area, we observe a NNW-SSE trending ductile–brittle shear zone (discussed later in chapter 3.4) cutting through the continuous exposure of the Jubrique unit (Fig. 2).

Away from the contact with the Ronda Peridotites, the upper part of the Jubrique metamorphic sequence is characterized by medium- to low-grade Gr-bearing dark schists and quartzites. These rocks are overlain by phyllite-quartzite and meta-carbonate rocks (Balanyá et al., 1997).

High-grade rocks of the Jubrique unit exhibit an increasing metamorphic grade toward the Ronda Peridotites, which reaches partial melting near the contact. Within the migmatitic domain, partial melting is more pronounced close to the peridotites, leading to the formation of more chaotic structures due to higher melting percentages, while stromatic metatexites are found upwards (Fig. 4A). The basal portion of the crustal section is dominated by Grt-bearing granoblastic gneisses (Fig. 4B). Blastomylonitic textures are common near the sheared contact with the mantle rocks.

Grt gneisses are banded rocks with alternating Bt + Sil-rich bands interlayered with centimeter-sized Qz-feldspathic domains. These rocks are characterized by the presence of prominent Grt porphyroblasts, measuring up to 1 cm in diameter and comprising up to 20 vol% of the rock. The mineral paragenesis in these gneisses and migmatites includes Qz + Kfs + Bt + Grt + Sil + Pl \pm Ky \pm Crd, where Sil replaces Ky, defining the main foliation, while Crd is part of Grt rims together with Bt + Qz (Fig. 4C). These observations are consistent with those of previous authors (e.g., Barich, 2015; Acosta-Vigil et al., 2016).

The Jubrique crustal rocks overlie the Spl \pm Grt mylonites and Spl tectonites domain of the Ronda Peridotites, which therefore represent the sheared top of the mantle section (Fig. 4D). At the contact, peridotites exhibit a high-grade ultramylonitic to mylonitic ultramafic assemblage, distinguished by the presence of rare Grt, Spl, and highly stretched pyroxene porphyroclasts, which stand out within the fine-grained groundmass. This groundmass is primarily composed of Ol grains measuring $< 200 \mu\text{m}$ in diameter. The high-T tectonic foliation and the compositional layering in these peridotites are sub-parallel to the contact with the overlying crustal units. North of Sierra Bermeja, pyroxenes indicate a lineation trending ENE-WSW, while to the south, it trends WNW-ESE (Fig. 2). These lineations show a significant correlation with those observed in the blastomylonitic gneisses overlying the ultramafic rocks (e.g., Balanyá et al., 1997).

The approximately 100 m-thick peridotite mylonitic domain is progressively replaced by Spl tectonites through the gradual increase in Ol grain size and the disappearance of Grt. Nevertheless, the Spl tectonite domain also exhibits compositional layering, which includes different peridotite lithologies and/or concordant Spl \pm Grt pyroxenite layers. These layers are parallel to the high-T tectonic foliation of the peridotites and the contact with the overlying crustal rocks. Compositionally, both mylonites and tectonites are predominantly harzburgites, along with some lherzolites and minor dunites. As consistently found in previous studies in the western part of the Ronda massif, the Spl tectonite domain in our study area is replaced by granular Spl peridotites across a relatively sharp contact, commonly referred to as the recrystallization or coarsening front in previous works (e.g., Van der Wal and Bodinier, 1996; Lenoir et al., 2001; Soustelle et al., 2009).

3.2. The Guadaiza unit and associated ultramafic rocks

The lithological sequence of the Guadaiza unit is best exposed in the central and northeastern regions of the study area, particularly in the Guadaiza river valley, as well as in the southern part of Sierra Bermeja, north of Istán and south of Ojén (Fig. 2). In contrast to the prevailing structural interpretation, however, our detailed field observations at the contact areas between the crustal and mantle rocks reveal that the Guadaiza crustal unit overlies the Ronda Peridotites (Fig. 3). Field evidence supporting the proposal for a revised structural position of peridotites include the following:

(i) peridotites are overlain by the basal members of the crustal unit in several outcrops. The heterogeneous granites, which record the highest degree of crustal anatexis at the base of the Guadaiza crustal sequence, clearly overlie the peridotites at Puerto del Robledal, located 2 km NW of the Guadaiza valley (Figs. 2 and 5A). A similar geological configuration is observed NE of Estepona, where marbles and migmatites overlie the peridotites (Figs. 2 and 5B), confirming previous observations by various authors (e.g., Loomis, 1972; Sanz de Galdeano and López Garrido, 2016; Torres-Roldán, 1983; Sanz de Galdeano, 2017). Regarding the Guadaiza river, peridotites and Guadaiza-type metatexites or schists show an almost vertical contact to the west of the valley, as to the east, although highly affected by late fragile structures,

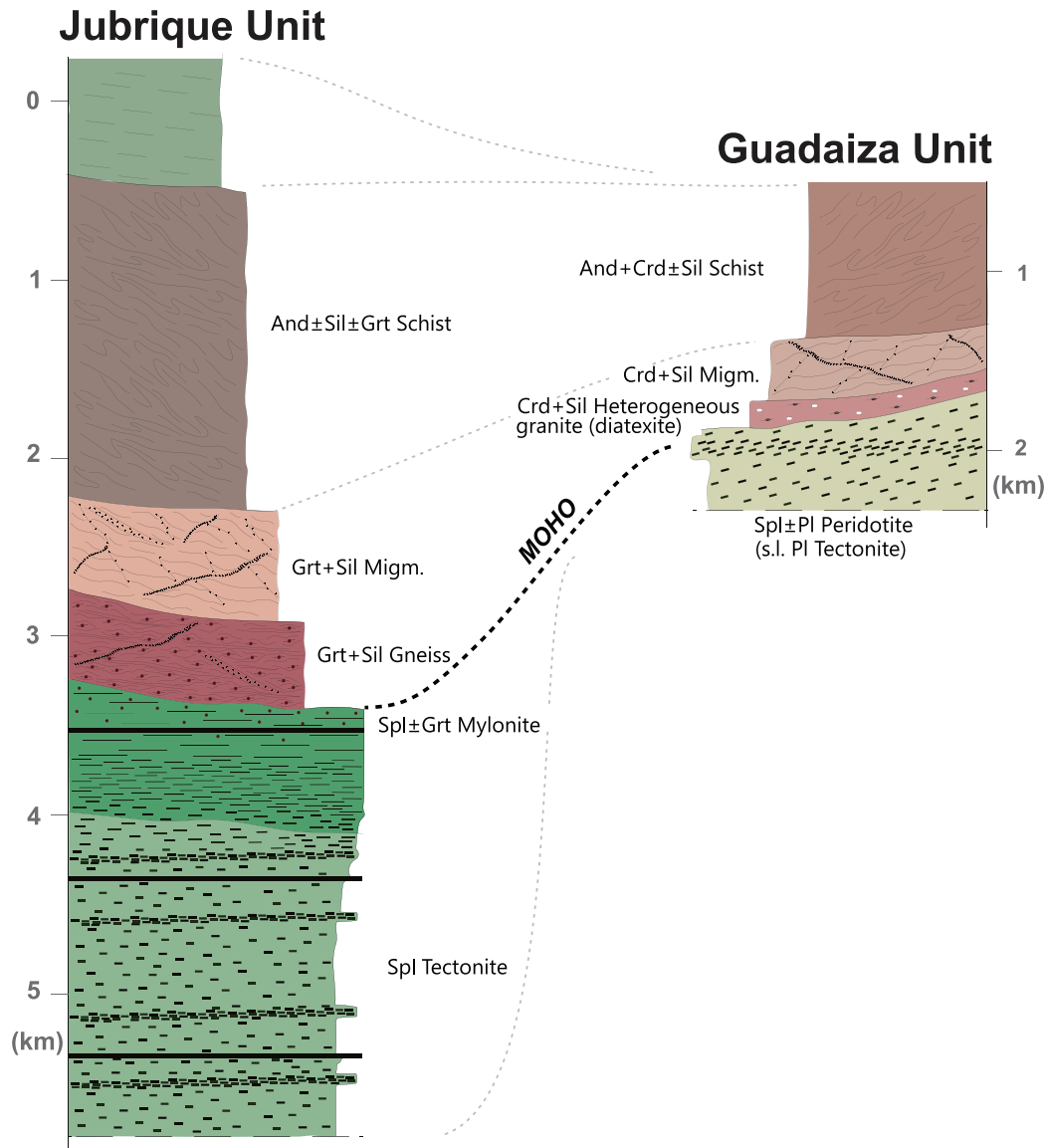


Fig. 3. Schematic lithospheric columns of the Jubrique and Guadaiza units. Total thickness was obtained from the cross-sections in the Fig. 2.

diatexites and heterogeneous granites overlay the ultramafic rocks through a high angle contact dipping to the west (Figs. 2 and 5C).

(ii) What previously was interpreted as the deformed metamorphic sole of peridotites thrusting over crustal units, termed as “migmatitic breccia”, is in fact undeformed heterogeneous granite (diatexite migmatite) at the base of the Guadaiza unit (Figs. 3, 6). The heterogeneous granites contain abundant restite clasts and schlierens, as expected for a diatexitic migmatite but, unlike proposed in earlier papers (Tubía et al., 1997, 2013), Pl tectonite peridotite fragments are rare, which would be otherwise common if this unit was indeed a basal thrust zone. Although both the metamorphic and ultramafic rocks in the Guadaiza section may locally exhibit high-T tectonic foliation (presented later in details, Fig. 6), the contact itself, unlike in the Jubrique unit, does not represent a discrete shear zone and is not associated with a shear gradient on either side.

(iii) Finally, the systematic exposure of heterogeneous granites with the Spl ± Pl peridotites domain across non-deformed contacts also excludes that these crustal rocks served as the metamorphic sole of a basal thrust, because in that case their juxtaposition with other tectonometamorphic domains would be also observed. In

fact, the Guadaiza heterogeneous granites are exposed with peridotites different to Pl tectonite only in the western portion of the study area, where the Guadaiza and Jubrique units, together with their associated ultramafic rocks are juxtaposed along a km-scale, NNW-SSE trending brittle-ductile shear zone (Fig. 2). However, this large-scale structure postdates the formation of the two types of crust-mantle contacts and will be presented in detail in section 3.4.

Nevertheless, it is important to note that late-stage high-angle reverse faults often result in local overthrusting of crustal units by mantle rocks (Fig. 5D). Some notable contacts of this type are: (i) in the northern part of the study area, mantle rocks associated with the Guadaiza unit overthrust the Triassic, shallow platform carbonate rocks of the Nieves Unit (Fig. 2), which belong to the Frontal Units (Martín-Algarra and Vera, 2004). Almost parallel to this major contact, a km-scale, south- to southeast-vergent thrust fault locates the Pl-tectonites over the heterogeneous granites to the north of the Guadaiza river (Figs. 2, 5C and D). However, along this type of fault contacts, the footwall rocks, often composed of migmatites or heterogeneous granites, remain relatively undisturbed, while the hanging wall peridotites show intense



Fig. 4. Field and microscope images (plane polarized light) of the lithologies that constitute the Jubrique lithospheric unit. A) Grt-migmatites. B) Grt-bearing granoblastic gneisses (kinzigites). C) Partially reabsorbed Grt porphyroblast rimmed by a Crd mass at the base of the Jubrique crustal unit. D) Petrological Moho exposed to the south of the Concepción reservoir (Fig. 2). The sheared contact presents here a high-angle attitude dipping to the southeast.

serpentinization associated with slickenlines and S-C textures consistent with reverse faulting (Fig. 5D), thus they are relatively straightforward to differentiate in the field.

The maximum thickness of the Guadaiza-type crust, including its corresponding portion of upper crust, is only 3 km. The uppermost part of the Guadaiza unit consists of dark schists, interbedded with quartzites, phyllites and marbles. The schists represent the lower grade domain of the metamorphic sequence and are characterized by a planar-linear fabric composed of rotated, pre-kinematic And porphyroblasts embedded in alternating Bt + Crd ± Sil and Qz-felspathic bands (Fig. 6A). The lineation defined by

elongated minerals shows a constant NNE-SSW azimuth, plunging approximately 10–30° to the south. Towards the contact with the Ronda Peridotites, the metasedimentary sequence becomes dominated by migmatites, which record varying degrees of partial melting, typically increasing close to the mantle rocks. In contrast to the Jubrique unit, the Guadaiza migmatitic and metamorphic parageneses are dominated by Crd masses grown within mafic bands, but also appearing as porphyroblasts in leucosomes and heterogeneous granites. The base of the Guadaiza section corresponds to these heterogeneous granites (Fig. 6B–E), which are in contact with the peridotites of the Pl tectonite domain. Transitional domains

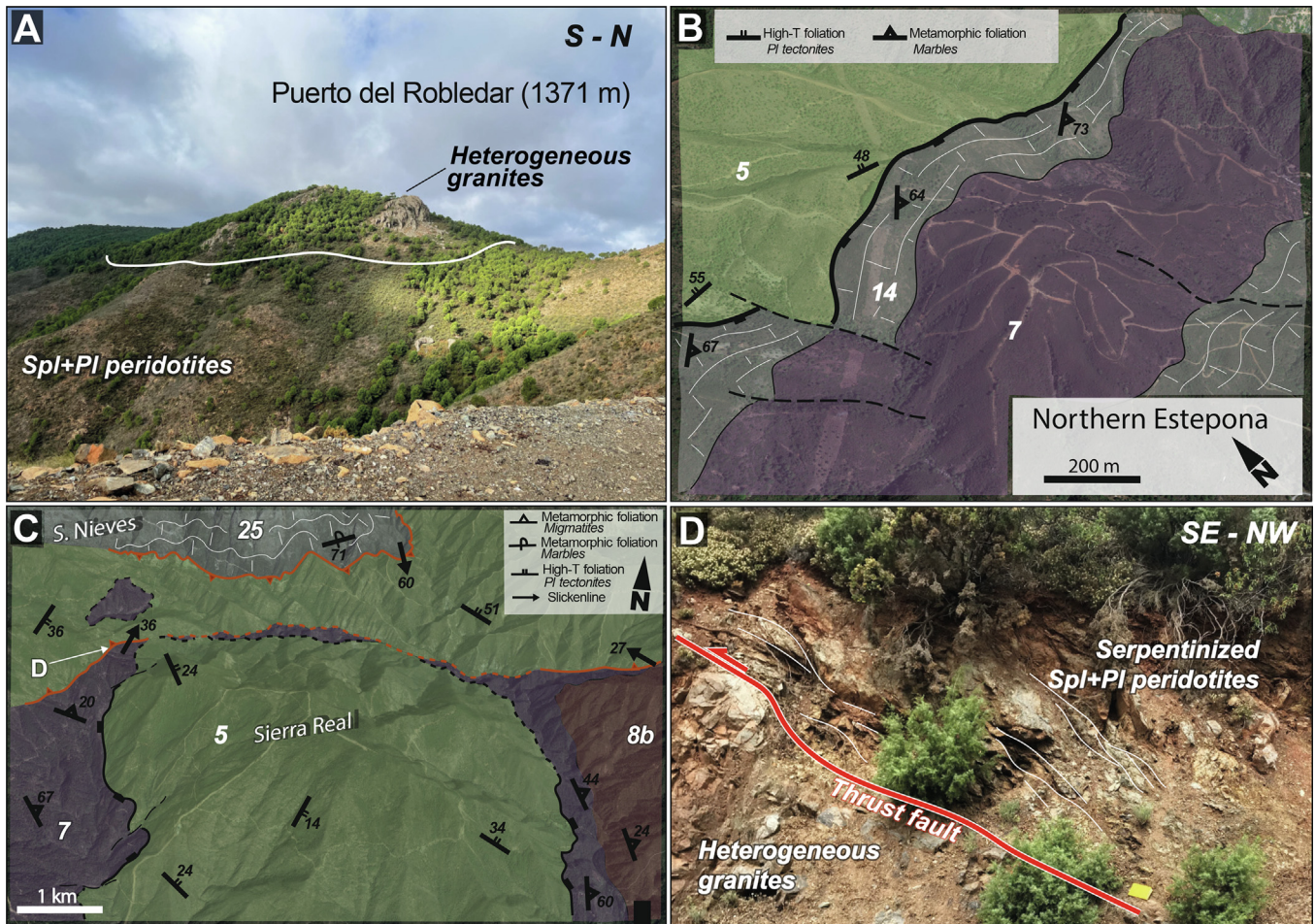


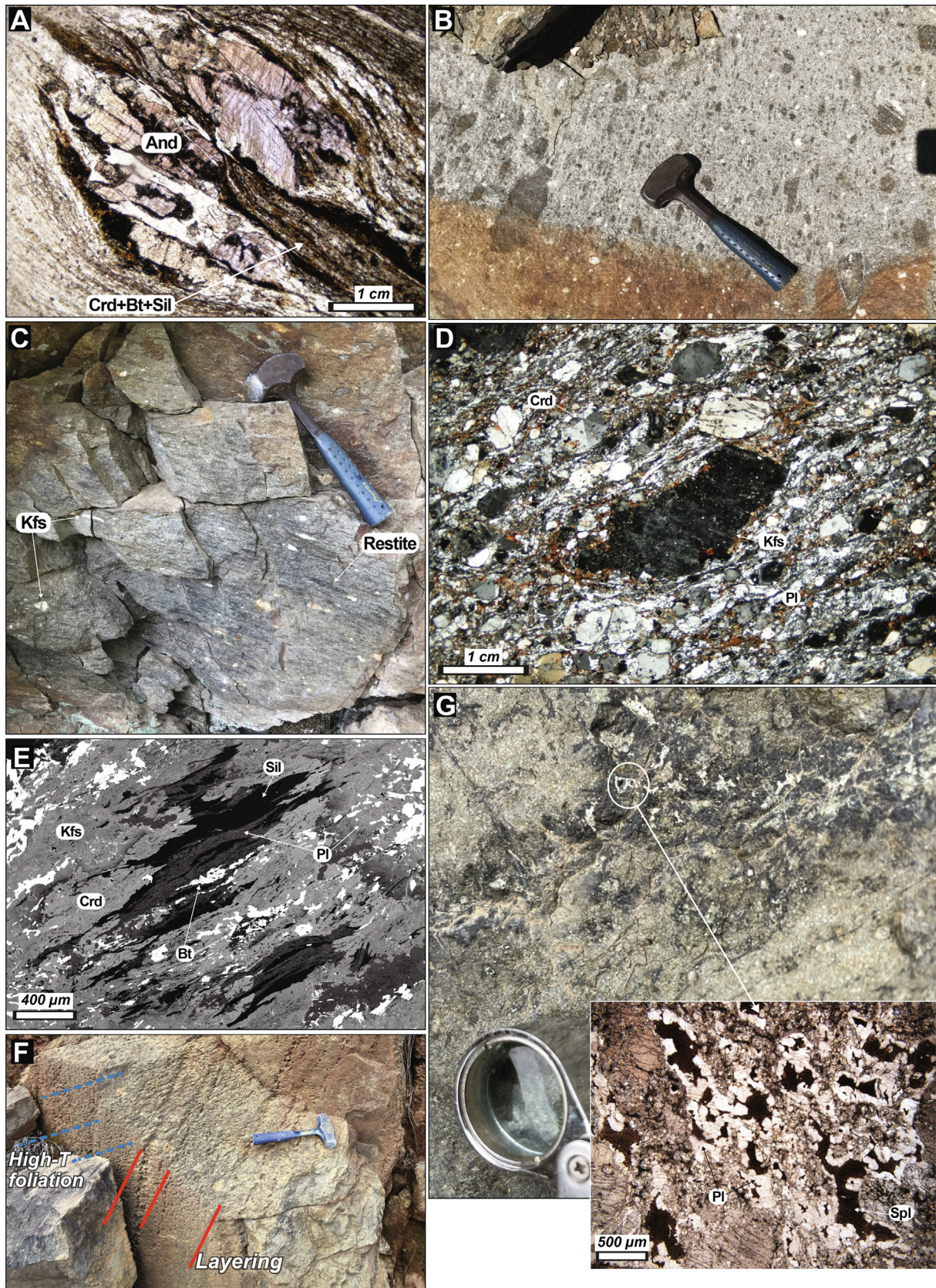
Fig. 5. Field photographs and satellite images showing the main contacts between peridotites and migmatites and marbles in the Guadaiza unit. A) Disposition of heterogeneous granites over the Spl + Pl peridotites to the north of the study area (Fig. 2). Close to the contact, both the orientation of flattened restites and the high-T foliation of the peridotites show a roughly N-S to NNE-SSW azimuth dipping to the west. B and C) Geological sketches of the contacts between Spl + Pl peridotites and high-grade marbles and heterogeneous granites to the north of Estepona (B) and to the north of the Guadaiza river (C) (Fig. 2). Numbers are referred to the lithologies in the Fig. 2. Primary contacts where Guadaiza units overlie the peridotites (black lines) contrast with thrust faults (red lines) that locate highly serpentized peridotites over the crustal rocks. D) Close sight to the thrust contacts between serpentized peridotites atop of the heterogeneous granites. See location in Fig. 5C. Peridotites show a fragile S-C structure and abundant slickenlines defining the reverse kinematics. (For interpretation of the references to colour in this figure legend, the reader is referred to the web version of this article.)

within the migmatites are characterized by the disaggregation of the stromatic structure of the metatexites, isolating bands and blocks of mesosome and melanosome with parasitic folds (restites) surrounded by transposed leucocratic domains. Some of these transitions might have been influenced by ductile shearing and late brittle faulting.

The basal heterogeneous granites of the Guadaiza unit (Fig. 3) are best exposed along the Guadaiza river valley and south of Ojén (Fig. 2). These granites, together with migmatites and schists, constitute the lower part of the crustal sequence and correspond to nebulitic diatexites. They are characterized by abundant Bt + Crd ± Sil restites and large Kfs nodules included in a granitic matrix (Fig. 6B and C). This lithology has been often referred to as “migmatitic breccia” by previous authors (e.g., Lundeen, 1978; Torres-Roldán, 1983; Tubía and Cuevas, 1986; Tubía et al., 1997, 2013; Esteban et al., 2008). The fragments of this false breccia locally display intense ductile deformation pattern with variably flattened rigid objects, such as restites, Qz restites and Kfs nodules (Fig. 6C). At microscopic scale, highly stretched Qz grains form a fine-grained ribbon texture surrounding Pl, Kfs and Crd porphyroclasts (Fig. 6D) and restites (Fig. 6E). At outcrop scale, the degree of apparent deformation in the heterogeneous granites is inversely

proportional to the size and distribution of the restites within the rock, i.e., increased deformation results in more homogeneous textures composed of finer-grained equigranular components within the diatexites. The stretched objects, mainly restites, Qz restites and Kfs nodules, and matrix constitute a planar fabric that shows a good correlation with the migmatitic banding and schistosity along the Guadaiza crustal sequence. In the study area, a remarkable strain gradient is observed in the area between the Sierra de las Nieves and Montemayor, close to the NNW-SSE trending km-scale brittle-ductile shear zone (see section 3.4). In this sector, the heterogeneous granites form medium-grade protomylonites and mylonites marked by completely recrystallized Qz and Kfs porphyroclasts, which display undulose extinction and core-mantle microstructures due to partial dynamic recrystallization. In a distance of 25–50 m from the core of the shear zone, a gradual transition is observed from mylonites to typical undeformed migmatites. Sheared granites form discrete bands in the migmatitic sequence (e.g., Guadaiza valley) (Fig. 2).

The mantle section beneath the Guadaiza unit is dominated by Spl ± Pl peridotites, which constitute the majority of the eastern and southern parts of the Ronda massif (Figs. 2 and 3). These lithologies exhibit two, rather irregularly intercalated subfacies of



varying scale (from deka- to hectometric) in the field: (i) Pl tectonites, and (ii) refractory, granular or porphyroclastic Spl peridotites. The Pl tectonites are porphyroclastic Pl-bearing Spl lherzolites characterized by the development of a pervasive, high-T tectonic foliation associated with the occurrence of sub-solidus Pl around Spl (Fig. 6F and G). Pyroxene porphyroclasts and Spl + Pl aggregates are stretched in the plane of the foliation (Fig. 6F). The second subfacies primarily comprises more refractory, Pl-free lithologies such as Ol-rich Spl lherzolite and Spl harzburgite, and, locally, dunite. Previous studies referred to such rocks as fine-granular peridotites and as a layered sequence of Ol-rich lherzolites, harzburgites and dunites (e.g., Remaïdi, 1993; Garrido and Bodinier, 1999). However, these rocks often display moderately elongated clusters of Spl and pyroxenes, along with individual porphyroclasts of the same minerals, which are aligned in a plane similar to the high-T foliation observed in the closest Pl tectonite outcrops. The mineral clusters and porphyroclasts are embedded within a relatively fine-grained Ol matrix, except for dunites, where Ol grain size varies considerably. Moreover, the fertile pyroxenite layers hosted within and around these refractory peridotites typically contain Pl as rims around Spl (cf. Obata, 1980; Garrido and Bodinier, 1999; Bodinier et al., 2008), and show a wide compositional variability including Spl ± Pl websterites, clino- and orthopyroxenites. Thus, we infer that the appearance of Pl in the refractory peridotites is controlled essentially by compositional heterogeneities in the whole rock. Consequently, despite the apparent lack of macroscopic Pl, the peridotites in the fine-granular subfacies, as well as in the layered sequence of refractory peridotites are indeed part of the Pl tectonite domain.

3.3. Other units

West of Sierra Blanca, migmatitic orthogneisses and leucogranites alternate with heterogeneous granites along the tectonic contact with the Spl ± Pl peridotites in the vicinity of Istán (Fig. 2). Field observations, estimated P-T conditions, and diagnostic parageneses link these orthogneisses and related leucogranites to the Guadaiza unit (Acosta-Vigil et al., 2014). The orthogneisses consist of interlayered Qz-feldspar and Bt-rich bands; elongated cm-scale Kfs porphyroclasts form part of the Qz-Kfs bands. As partially melted rocks, they enclose two types of leucosomes: (i) concordant, Grt-rich leucogranitic layers parallel to the gneissic foliation, and (ii) irregular blobs and dikes of Crd leucogranites that crosscut the foliation. The volume of leucogranites increases towards the contact with the peridotites (westward, Fig. 2), where the orthogneisses progressively lose their primary structure and transform into a restite-rich leucogranitic domain. In this area, leucogranites and heterogeneous granites show lobulate magma-magma contacts and present self-intrusive relationships.

Marbles constitute a significant component of the continental sequences overlying the Ronda Peridotites. In the area around Montemayor and in the Guadaiza river valley, they form several m-thick bands, which are interleaved and deformed together with migmatites and heterogeneous granites of the Guadaiza unit. These

marbles are coarse-grained banded rocks frequently displaying minor structures, such as asymmetric microfolding and shear bands. They contain abundant Phl, Tr, Di and/or Fo, among other Ca- and Mg-rich minerals. Furthermore, to the east of the study area, the Ojén unit can be distinguished by the voluminous massifs of high-grade marbles (Fig. 2). The condensed section of migmatites and schists of the unit appears overturned and overlying the marbles. The Sierra Blanca consists of a lower unit comprising white dolomitic marble, and an upper unit composed of banded carbonates interlayered with metapelitic and amphibolitic bands. Some authors have proposed a Triassic age for these marbles based on their correlation with Alpujárride sequences from the central part of the cordillera (e.g. Braga and Martin, 1987). However, given the structural correspondence and continuity with migmatites, it has also been suggested that they originated from a Paleozoic protolith that underwent a Permo-Triassic metamorphism (Fig. 2).

Finally, in certain sections, we have observed a gradual transition from the lowermost Maláguide formation, namely the Morales Formation, to the underlying uppermost Alpujárride phyllite and quartzite sequence. This transitional zone is observable in road cuts between Istán and the coast, as well as between Estepona and Peñas Blancas (Fig. 2). In these exposures, the Morales Formation, characterized by alternating layers of shale and greywacke, grades into Alpujárride phyllites and quartzites downwards.

3.4. Large-scale tectonic structures

The geological map reveals two, brittle-ductile, km-scale, anastomosing NNW-SSE and ENE-WSW trending discrete shear zones. The NNW-SSE trending Igualeja-Benahavís shear zone divides the peridotite massif, extending from the Sierra de las Nieves to the Montemayor sector (Fig. 2). As for the ENE-WSW trending shear zone, it runs parallel to the coastline south of Sierra Bermeja along the southern part of the study area. In general, the Guadaiza-type units are found to the east of the NNW-SSE shear zone and north of the ENE-WSW one.

The NNW-SSE oriented shear zone comprises high-angle (60–70°) westward-dipping narrow bands that crosscut both crustal and mantle units. The affected crustal rocks are dominated by heterogeneous granites and metatexite migmatites, which develop brittle-ductile mylonitic fabric in the plane of the shear zone foliation. Away from the shear zone, mylonitic fabric is not observed in the migmatitic crustal sequence. Within the peridotites, deformation is primarily localized into up to a few cm-thick serpentinized faults, while the high-T microstructure of peridotite host rock remains unaffected. In the vicinity of the shear zone, ultramafic rocks are usually intensely serpentinized. The ENE-WSW oriented shear zone is characterized by high-angle (>70°), dominantly southward-dipping foliation, but it is noteworthy that most shear zones have been potentially reactivated under contractional conditions during Alpine times. Consequently, the ENE-WSW segments experienced brittle reactivation as high-angle reverse faults. Cross-cutting relationships indicate that the Aquitanian leucogranite dikes intruded during the brittle deformation event, likely also

Fig. 6. Field and microscope images of the lithologies that constitute the Guadaiza lithospheric unit. A) Rotated pre-kinematic And porphyroblasts surrounded by the schist foliation defined by Bt + Sil + Qz + Pl + Kfs and embedded in a Crd mass (plane polarized light). B) Heterogeneous granites (diatexites) composed of abundant restites and Kfs nodules in a Qz + Pl + Kfs + Crd matrix. The long axes of the restites define an incipient orientation. C) Heterogeneous granites showing an intense ductile fabric constituted by flattened restites and Kfs nodules. Note the reduced size of the stretched objects and the more homogenous texture of the rock compared to less deformed diatexites (Fig. 5B). These rocks constitute discrete, ductile shear zones in inner areas of the Guadaiza migmatites, without a strain gradient towards the contacts with mantle rocks. D) Microstructure of the sheared heterogeneous granites. Fine-grained Qz ribbons and Bt flakes surround Crd, Pl and Kfs crystals, the latter showing high-T, plastic deformation (crossed polarized light). E) BSE image of a restite in the heterogeneous granites. Note the scarce presence of fine-grained Bt included in the Crd mass. F) Spl + Pl peridotites showing the typical oblique disposition of the compositional layering and the high-T foliation. G) Abundant Pl surrounding Spl in Pl tectonites of the Guadaiza unit (plane polarized light).

Table 1
List of studied samples from the crustal units overlying the Ronda Peridotites.

Rock type	Sample	Location		Unit	Study area	Methods				
		X	Y			WR-G	M–G (P-T)	Geochr		
Kinzigite (Grt-gneiss)	Knz-1	30S 304,386	E 4,048,334	Jubrique	Jubrique	X				
	Knz-3	30S 323,149	E 4,045,170		Real de la Quinta	X				
	Knz-6	30S 313,882	E 4,042,651		Montemayor	X				
	Heterogeneous granite (Diatexite)	GH-1	30S 312,659	E 4,042,350	Guadaiza	La Resinera	X	X		
		GH-2	30S 314,257	E 4,042,892		Montemayor	X	X		
		GH-3	30S 314,401	E 4,044,493		Montemayor	X			
		GH-4	30S 321,663	E 4,046,117		Guadaiza S	X			
		GH-5	30S 316,831	E 4,056,566		S. Las Nieves	X			
		GH-6	30S 319,881	E 4,055,294		Guadaiza N	X			
		GH-8	30S 326,092	E 4,052,083		Istán	X			
GH-9		30S 314,297	E 4,043,568	Montemayor		X				
GHc-1		30S 321,006	E 4,053,641	Guadaiza E		X				
GHc-3		30S 322,290	E 4,049,130	Guadaiza E		X				
Migmatite	SN-18	30S 313,195	E 4,045,768	Jubrique	La Resinera			X		
	MA-07	30S 320,961	E 4,045,667		Guadaiza			X		
	SN-62	30S 313,359	E 4,054,582		S. Las Nieves			X		
	SN-67	30S 314,219	E 4,043,193		Montemayor			X		
	MA-05	30S 318,510	E 4,041,264		Benahavís			X		
	OJ-02	30S 334,837	E 4,051,184		Ojén	X		X		
	Gneiss	Gnlst-1	30S 325,614		E 4,049,828	Guadaiza	Istán	X		X
		Gnlst-2	30S 326,671		E 4,051,624		Istán	X		
		Gnlst-3	30S 326,210		E 4,052,392		Istán	X		
	Leucogranite	Lclst-1	30S 325,478		E 4,049,865		Istán	X		
Lclst-2		30S 326,662	E 4,051,617	Istán	X					
Lclst-3		30S 325,807	E 4,052,030	Istán	X					
Schist	Scht-1	30S 303,394	E 4,048,425	Jubrique	Jubrique	X				
	Scht-2	30S 320,326	E 4,045,820	Guadaiza	Guadaiza	X	X			
	Scht-3	30S 326,028	E 4,049,886	Guadaiza	Istán	X				
	Scht-5	30S 332,294	E 4,055,131	Guadaiza	Monda	X				

WR-G: whole-rock geochemistry

M–G (P-T): Mineral geochemistry. Thermobarometric calculations

Geochr: Geochronology

accompanied by the circulation of fluids associated with serpentinization of peridotites (e.g. Pedrera et al., 2016).

4. Methods

4.1. Sampling strategy and sample preparation

Rock types, sample locations and methods are shown in Table 1. Sampling was carried out to cover the different crustal units that overlie mantle peridotites across the study area. Altogether, 29 samples have been included in this study, of which 24 were analyzed for whole rock geochemical composition, three (one schist and two diatexites) were used to analyze mineral compositions and to obtain thermobarometric calculations in the Guadaiza-type lower crustal units, and seven (migmatites and heterogeneous granites) were processed for geochronology.

4.2. Geochemistry

Approximately 5 kg of fresh rock was collected from each sample of lower crustal units, migmatites and schists analyzed for the geochemical study (Fig. 2; Table 1). Major and trace element compositions of analyzed samples are presented in Supplementary Material 1. Samples were crushed and milled to a fine powder for whole-rock geochemistry. Major elements and Zr were determined by X-ray fluorescence (XRF) at the CIC-UGR (Centro de Instrumentación Científica, University of Granada, Spain). Precision for major elements is better than 1 % relative. Trace elements, except for Zr, were obtained by inductively coupled plasma mass spectrometry (ICP-MS) at the CIC, University of Granada, following the standard procedures described by Baedeker (1987). Analysis of trace elements was carried out according to the method

described by Bea et al. (1996); the precision was approximately 2 % and 5 % error on concentrations of 50 and 5 ppm, respectively.

Polished thin sections of two diatexites (heterogeneous granites) were analyzed to determine the mineral major element composition using a JEOL JXA-8200 Superprobe at the University of Huelva (Spain). A combination of silicates and oxides were used for calibration. A beam of 5- μ m diameter was used to analyze mineral phases to minimize Na migration. Averaged mineral compositions of analyzed phases are presented in Supplementary Material 2.

4.3. Radiometric dating

Zircon separation was accomplished by traditional techniques using dense liquids and magnetic separation (Frantz) at the University of Huelva. Crystals free of impurities and fractures were selected by hand-picking under a binocular microscope. Analyses were carried out in the SHRIMP II microprobe at the IBERSIMS laboratory (CIC-UGR, University of Granada). Zircon concentrates were cast on a 3.5 cm diameter epoxy mount, together with zircon standards (TEMORA, SL13 and GAL zircon) and documented by a Zeiss EVO-150 SEM equipped with a cathodoluminescence detector (SEM-CL). Mounts were coated with gold (80- μ m thick) and inserted into the SHRIMP for analysis. Each selected spot was rastered with the primary beam during 120 s prior to analysis, and then analyzed over 6 scans following the isotope peak sequence: $^{196}\text{Zr}_2\text{O}$, ^{204}Pb , 204.1 background, ^{206}Pb , ^{207}Pb , ^{208}Pb , ^{238}U , ^{248}ThO , ^{254}UO . Every peak of each scan was measured sequentially 10 times with the following total counts per scan: 2 s for mass 196; 5 s for masses 238, 248, and 254; 15 s for masses 204, 206, and 208; and 20 s for mass 207. The primary beam, composed of $^{16}\text{O}^{16}\text{O}^{2+}$, was set to an intensity of 4 to 5 nA, using a 120- μ m

Kohler aperture, which generates $17 \times 20\text{-}\mu\text{m}$ elliptical spots on the target. The secondary beam exit slit was fixed at $80\ \mu\text{m}$, reaching a resolution of about 5000 at 1 % peak height. Mass calibration was carried out on the GAL zircon (ca. 480 Ma, very high U, Th and common lead content; [Montero et al., 2008](#)). Sessions initially involved the measurement of SL13 zircon ([Claoue-Long et al., 1995](#)), used as a concentration standard (238 ppm U). TEMORA zircon (ca. 417 Ma, [Black et al., 2003](#)), used as isotope ratios standard, was measured every 4 unknowns. The final result for each isotope was calculated as the value at the mid-time of the analysis resulting from the regression line. $^{206}\text{Pb}/^{238}\text{U}$ was estimated from the measured $^{206}\text{Pb}^+/^{238}\text{U}^+$ and UO^+/U^+ , following the method of [Williams \(1998\)](#). Plotted and tabulated analytical uncertainties are 1σ precision estimates. U–Th–Pb geochronological results (U, Th and Pb contents, isotopic ratios, ages and analytical uncertainties) are shown in [Supplementary Material 3](#) and CL images of zircons with spot locations are presented in [Supplementary Material 4](#). Concordia diagrams were obtained with ISOPLOT software ([Ludwig, 2003](#)). Uncertainties are 95 % confidence limits ($t\sigma$, where t is the student's t multiplier) and include the uncertainty in the Pb/U calibration (ca. 0.3–0.5 %). Ages were calculated using the constants recommended by the IUGS Subcommittee on Geochronology ([Steiger and Jäger, 1977](#)).

4.4. Thermodynamic modeling

Phase relations (P–T and T–X pseudosections) for the whole rock composition of the Guadaiza schists were calculated using the thermodynamic database ds62 ([Holland and Powell, 2011](#)) and the updated activity composition models (A–X) for all minerals and granitic melt, excluding feldspars ([White et al., 2014a](#)), with *Perple_X* (6.8.9; [Connolly and Petrin, 2002](#)) and *Thermocalc* (TC-350; [Powell et al., 1998](#)). In both calculations, the same A–X models were used on the Scht-2 sample, which is representative of the Guadaiza schists. Considering the presence of Bt in these rocks, water content was selected to balance a modal 50 % of biotite (H_2O : 1–1.1 wt% \approx 4 mol%) together with reducing conditions given the absence of Mag ($O = 0.02$ mol%).

Potential errors due to analytical uncertainties are addressed in control calculations using half the measured MnO content (0.03 mol%). In these tests, we have also used for comparative purposes an earlier thermodynamic database (ds55; [Holland and Powell, 1998](#)), as well as the hCrd solution model for Crd (*Perple_X* ideal mixing model) and the Bio(TCC) solution model for Bt ([Tajčmanová et al., 2009](#)) with *Perple_X*, in order to check the influence of other A–X models in the stability curves for these minerals.

Phase relations and thermobarometric conditions prevailing during the formation of diatexites are addressed in two samples from the Guadaiza unit, using the whole rock composition and mineral geochemistry of GH-1 and GH-2 heterogeneous granites.

Additional P–T pseudosections were calculated under the same procedures for the Jubrique migmatites and Guadaiza heterogeneous granites (diatexites) and are presented as [Supplementary Materials 5 and 6](#) respectively.

5. Petrography and geochemical composition

5.1. Jubrique-type crustal units

The Jubrique unit ([Fig. 3](#)) shows a decreasing metamorphic grade from the contact with the ultramafic rocks upwards. The mineral paragenesis in the Grt gneiss is composed of $\text{Qz} + \text{Kfs} + \text{Bt} + \text{Grt} + \text{Sil} + \text{Pl} \pm \text{Ky} \pm \text{Crd}$. Kyanite is transformed into Sil, which, in turn, defines the main foliation. Cordierite is scarce and replaces Grt ([Fig. 4C](#)). Garnet porphyroblasts (up to 1 cm in diameter) are

typically euhedral or moderately elongated parallel to the foliation. The migmatitic lithologies are characterized by the lack of Crd, as well as the coexistence of Sil with Grt in leucocratic bands that mark the foliation.

The overlying gray and ochre schists are characterized by abundant Qz-rich bands and show polymorphic transformation of Sil to And at medium-grade outcrops located far from the migmatitic gneisses.

5.2. Guadaiza-type crustal units

The Guadaiza dark schists are dominated by And, Crd, and occasionally minor Sil. Garnet is scarce and pre-kinematic compared to the Jubrique unit. The Guadaiza schists exhibit a foliation (schistosity), which affects all of the minerals present in the samples. The texture of the schists is lepidoblastic–porphyroblastic. Various layers within the schists consist of Qz- and mica-rich domains, which could be associated with the original sedimentary layering. The mineral assemblage of the schists primarily comprises $\text{Qz} + \text{Bt} + \text{And} + \text{Ser} \pm \text{Grt} \pm \text{Pl} \pm \text{Kfs} \pm \text{Sil} \pm \text{Chl}$ in varying amounts. Quartz and Bt ($\pm \text{Sil}$, $\pm \text{Kfs}$) are syn-kinematic and contribute to the development of the observed planar fabric. Andalusite forms porphyroblasts within the schists and exhibits both pre-kinematic and syn-kinematic features. In some cases, clear strain shadows are absent, and the foliation wraps around the And crystals, which also display oriented inclusion trails ([Fig. 6A](#)). Garnet forms pre-kinematic porphyroblasts and exhibits strain shadows filled with Qz. Many of these Grt exhibit irregular morphologies and embayments, indicating dissolution processes. Sericite replaces Kfs, and some layers of Bt undergo chloritization. A detailed description of the mineralogy and textures observed in Guadaiza heterogeneous granites (see [Fig. 6](#)) was presented in [section 3.2](#).

5.3. Geochemical composition of the crustal rocks in the Guadaiza and Jubrique units

The Guadaiza schists (e.g., sample Scht-2) are of intermediate-felsic composition ($\text{SiO}_2 \approx 59$ wt%) with elevated contents in Al_2O_3 (20.65 wt%) and TiO_2 (1.39 wt%), and moderate/high concentrations of Na_2O (1.58 wt%), K_2O (3.39 wt%) and P_2O_5 (0.18 wt%). These rocks also show high A/CNK (2.79) and $\text{FeOt}/\text{MgO} + \text{FeOt}$ (0.83) molar and mass ratios respectively and can be classified as a shale using the $\text{SiO}_2/\text{Al}_2\text{O}_3$ vs. $\text{FeOt}/\text{K}_2\text{O}$ classification ([Herron, 1988](#)); where FeOt corresponds to all iron expressed as ferrous oxide. The Guadaiza heterogeneous granites (diatexites; e.g., samples GH-1 and GH-2) have felsic composition ($\text{SiO}_2 = 69.5$ wt% average), with relatively high CaO (0.84 wt% avg) and moderate contents in Na_2O (1.93 wt% avg), P_2O_5 (0.18 wt% avg), Al_2O_3 (14.80 wt% avg), TiO_2 (0.66 wt% avg) and K_2O (3.15 wt% avg) ([Supplementary Material 1](#)). They are highly peraluminous but less than the schists ($\text{A}/\text{CNK} = 1.80$), whereas their $\text{FeOt}/(\text{FeOt} + \text{MgO})$ is similar (0.79 avg). Based on the Ab–An–Or classification ([O'Connor 1965](#)) these rocks have an overall granitic composition.

The Jubrique schists (e.g., sample Scht-1) have intermediate-felsic SiO_2 contents (≈ 59 wt%) but their overall composition is more mafic due to higher MgO (2.3 wt%) and CaO (2.81 wt%) contents. Moreover, their P_2O_5 contents are noticeably elevated (0.27 wt%) compared to the Guadaiza schists ([Supplementary Material 1](#)). This rock type is also less peraluminous ($\text{A}/\text{CNK} = 1.36$) and has lower $\text{FeOt}/(\text{FeOt} + \text{MgO})$ values (0.75). Its classification based on the $\text{SiO}_2/\text{Al}_2\text{O}_3$ vs. $\text{FeOt}/\text{K}_2\text{O}$ mass ratios ([Herron, 1988](#)) is intermediate between shale and greywacke. The partially migmatized Jubrique kinzingite gneisses (e.g., samples Knz-1, Knz-3) have moderately felsic compositions ($\text{SiO}_2 = 63.58$ wt% avg) but with relatively elevated contents in

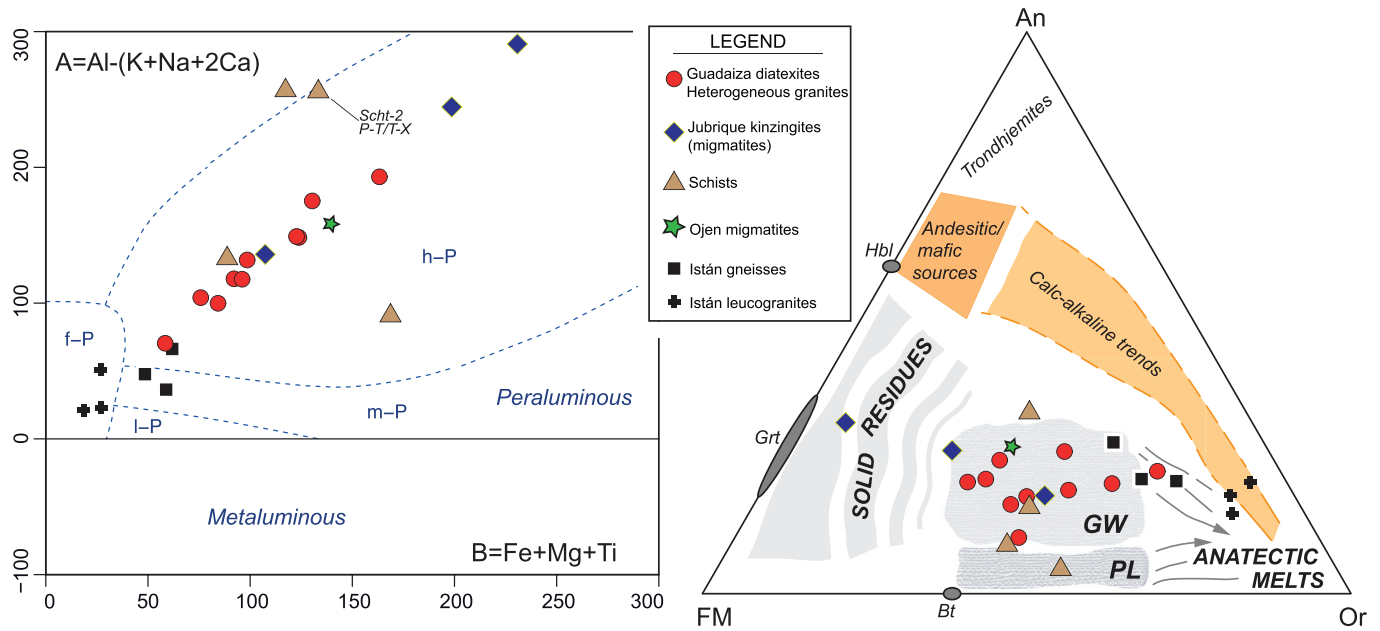


Fig. 7. Major elements geochemical projections. Besides the migmatites/kinzingites and diatexites/heterogenous granites of the Jubrique and Guadaiza crustal units, other regional metamorphic rocks have been plotted for comparison: Istán gneisses/leucogranites, Ojén migmatites and schists from different locations of the study area (Table 1). A) B-A classification diagram for granites from Villaseca et al. (1998). The indicated P-T/X point refers to the Schst-2 sample used for thermobarometric calculations. B) Projection of the studied samples into the pseudoternary system defined by Opx (FM)-Or (K)-An (Ca) (Díaz-Alvarado et al., 2011; Castro, 2013). Projections points are Qz, Ilm, Als, Ab, H₂O, FeMg-1 and FeMn-1.

TiO₂ (1.03 wt% avg), MgO (2.01 wt% avg), CaO (1.41 wt% avg) and MnO (0.14 wt%). They exhibit a characteristic low P₂O₅ (0.12 wt% avg) content, while the peraluminosity (A/CNK = 2.90) and the FeOt/(FeOt + MgO) mass ratio (0.81 avg) are both elevated. The Ab-An-Or classification (O'Connor 1965) for these rocks shows granitic, granodioritic and Qz-monzonitic compositions.

The variation of peraluminosity vs. maficity of Guadaiza and Jubrique samples can be observed in the A-B diagram (Fig. 7A; Villaseca et al., 1998). Other metamorphic rocks of the study area (e.g., Ojén migmatites, Monda schists and Istán schist and gneisses) have been also plotted in this diagram. The

Guadaiza schists show elevated A values (peraluminosity) and moderate to high B values (maficity). Other metamorphic rocks such as the Istán gneisses and leucogranites show lower values of both A and B parameters, close or in the field of felsic peraluminous granites. Most of the heterogeneous granites and kinzingite gneisses (Guadaiza and Jubrique respectively) define a positive correlation line, typical of rocks generated by partial melting of pelitic ± greywacke rocks and peritectic entrainment of Grt, Crd, and Sil. Some of the samples with higher A and B values could be enriched in peritectic/residual phases (Jubrique). Similar trends are observed in the FM-An-Or projection (Fig. 7B), which

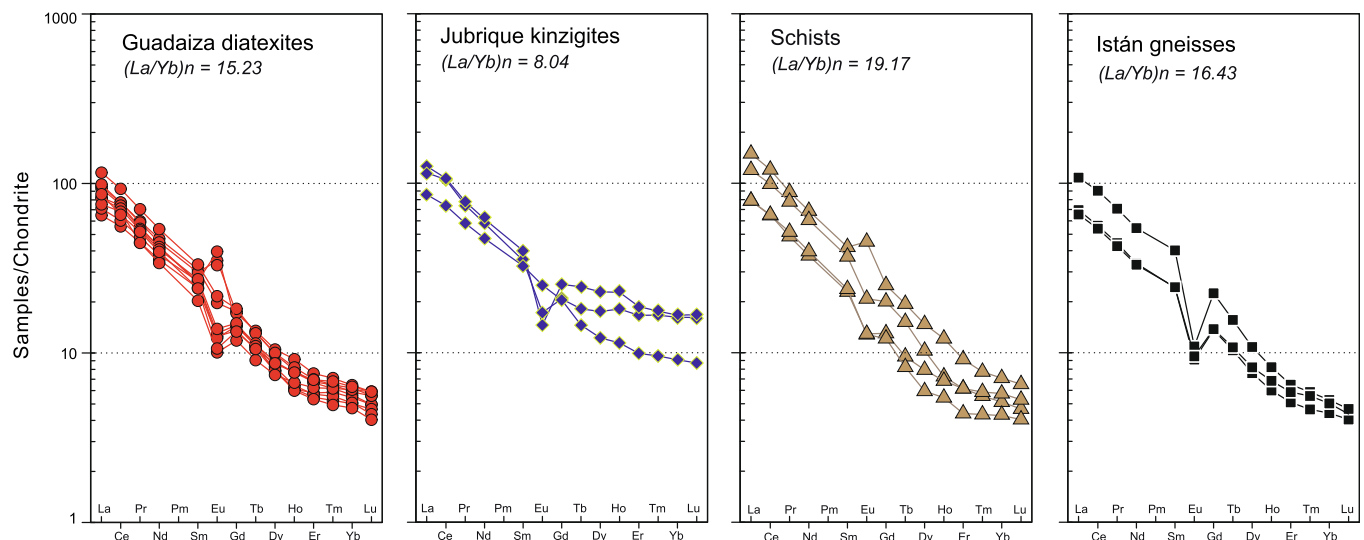


Fig. 8. Chondrite normalized REE diagrams for the Guadaiza and Jubrique crustal units (schists, migmatites/kinzingites, diatexites/heterogenous granites) and other metamorphic rocks in the studied zone. Chondrite REE contents taken from Boynton (1984). Note the elevated fractionation patterns in all the cases except for the Jubrique migmatites-kinzingites. See text for further details.

represents the variation of Fe-Mg, Ca and K components for sources and melts during partial melting processes (Castro, 2013; Díaz-Alvarado et al., 2011). Heterogeneous granites present short-range variations and fall in the field of greywackes and pelites, with few samples showing more restitic or leucogranitic compositions. In turn, the presence of large amounts of Grt and other metamorphic minerals in Jubrique kinzigites is depicted by the increase of FeO, MgO and Al₂O₃ in some of these samples. Schists present variable Al and Ca compositions and range between the fields of greywackes and pelites.

Trace element compositions of schists are characterized by high V and Ba and moderate Zr and Sr contents (Supplementary Material 1). Regarding rare earth elements (REE), metasedimentary rocks that overlie migmatites in Guadaiza and Jubrique crustal sections show very fractionated normalized REE patterns, both in light and heavy REE, (reaching HREE < 10× chondrite) compared to standard shales (Fig. 8). Although small, both positive and negative anomalies are observed in Eu. The Guadaiza heterogeneous granites have lower V (75 ppm avg), Zr (195 ppm avg), Ba (229 ppm avg) and Sr (88 ppm avg) contents. Their REE content, fractionation (La/Yb = 15.23) and general pattern are similar to those of the regional schists (Fig. 8). The Jubrique Grt-gneisses have similar trace element compositions to the studied Jubrique schists. REE patterns are fractionated only in the LREE while the MREE-HREEs present a relatively flat pattern, yielding a lower La/Yb ratio (8.04 avg) (Fig. 8). REE contents of Istán gneisses show similar fractionated patterns with more pronounced negative Eu anomalies.

To gain insight into the sources of the migmatites, gneisses or heterogeneous granites in the Jubrique and Guadaiza units, we have used major and trace element ratios to compare with standard and experimental compositions (Patiño-Douce, 1995; Altherr et al., 2000; Sylvester, 1998) (Fig. 9). The projected samples show that the Guadaiza migmatites could be derived from partial melting of metagreywacke with metapelite components, having similar geochemical composition to the studied schists. On the other hand, the Jubrique migmatites have lower Al₂O₃/[MgO + FeO], Rb/Ba and Rb/Sr values, that could indicate a metagreywacke source with relatively more mafic composition. The gneisses and leucogneisses from Istán are compatible with melts derived from pure metapelite-type sources. However, they are

typically considered the result of the metamorphism and partial melting of granitic rocks (Acosta-Vigil, 1998; Acosta-Vigil et al., 2014).

6. Thermobarometric conditions of crustal units

6.1. The Guadaiza unit

6.1.1. P-T pseudosections

The pseudosection calculated from the composition of Scht-2 schist (Fig. 10) is similar to those obtained in the Jubrique gneisses and migmatites in previous studies (e.g., Barich et al., 2014), and in the Guadaiza diatexites (Supplementary Material 5 and 6). Calculations indicate a wide stability field of Grt that is only not stable at pressures below approximately 0.35 GPa. K-feldspar and Pl remain stable under the investigated pressure-temperature conditions, at which either Sil or And are also stable, while Spl is present only in the high-T/low-P assemblages.

Calculated isopleths show that the melt percentages remain moderate/low (<15 %) with a low gradient at temperatures below 720–750 °C for the pressure range of 0.2–0.6 GPa. Both the amount and melting gradient increase surpassing the Bt-out curve with the dehydration-melting reaction: Bt + Sil + Pl + Qz → Kfs + melt + (Crd/Grt).

An important observation is that the current mineral assemblage in these schists (Bt + And/Sil + Grt + Qz + Pl/Kfs) cannot coexist within any of the calculated P-T fields. The pseudosection indicates that the rock underwent evolution from the subsolidus Grt-present field to the andalusite/sillimanite field at pressures below 0.3–0.4 GPa with an inferred decompression path. This agrees with the observed Grt dissolution features that indicates that this phase was more out of equilibrium compared to others. Moreover, the replacement of And by Sil (Fig. 6A) points to a T increase at pressures approximately 0.25–0.35 GPa.

The assemblage observed in the Guadaiza heterogeneous granites (diatexites), composed of Bt + Crd + Sil coexisting with melt (±Kfs) (Fig. 6), coexists in the pseudosection at 675–710 °C and 0.25–0.32 GPa (Fig. 10). Melt percentages calculated in this field vary between approximately 6–11 %. These values can increase

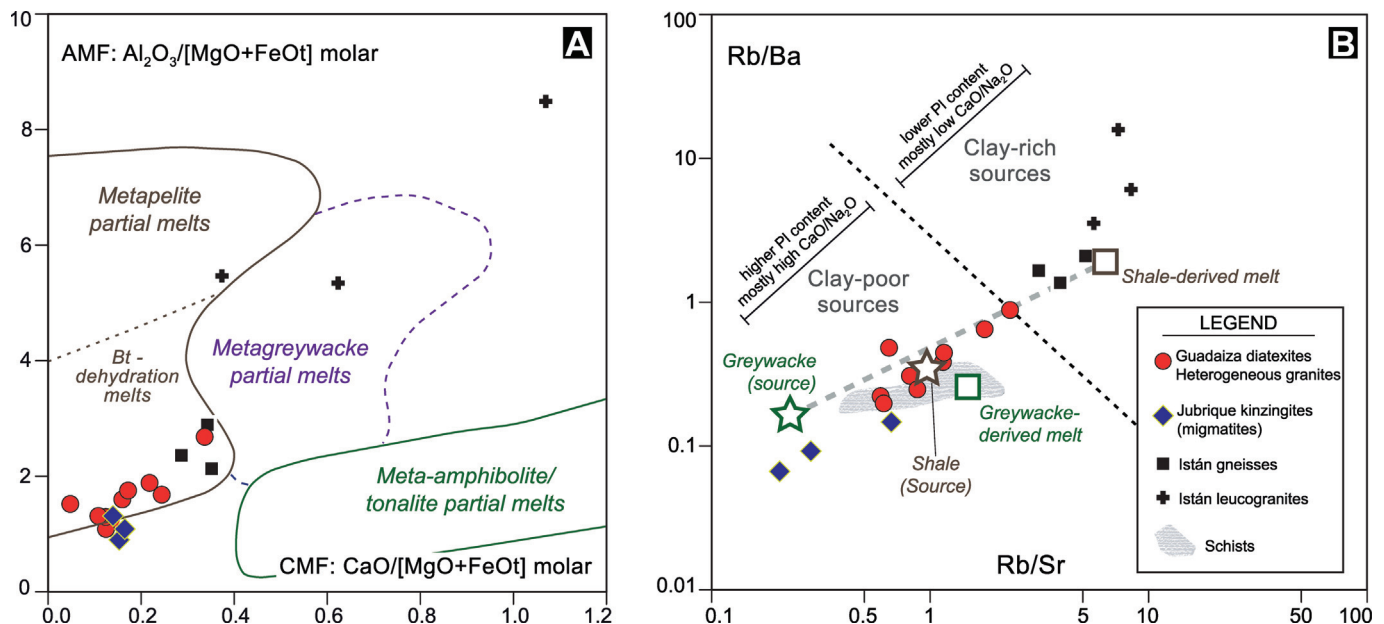


Fig. 9. A) Diagram for major element ratios (AMF, CMF) and fields for experimental melts based on Patiño-Douce (1995) and Altherr et al. (2000). B) Rb/Sr vs. Rb/Ba diagram for metasedimentary. Source compositions (Sylvester, 1998). Studied schist are projected in the shaded field

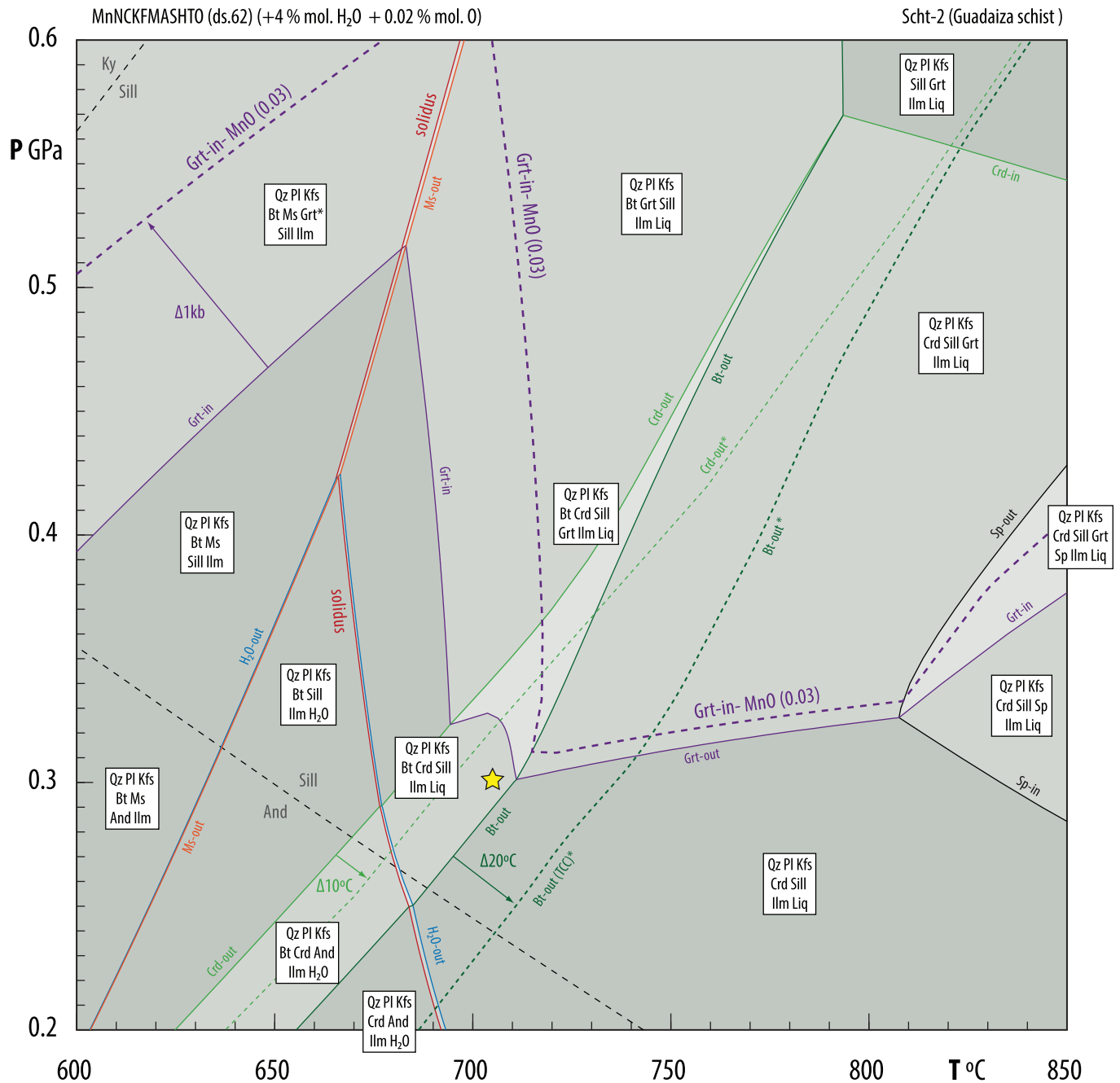


Fig. 10. P-T pseudosection of the Guadaiza schist (Sch2 sample). Grt-in curve at MnO = 0.03 mol% is shown in purple dashed line. Crd and Bt curves based on older A-X models are shown in green dashed lines. Mineral/phase abbreviations according to Whitney and Evans (2010). The yellow star shows the following modal assemblage coexisting with 9–10% of melt (Liq): Qz (20%) + Kfs (19%) + Pl (12%) + Crd (26%) + Bt (5%) + Sil (7%) + Ilm (1%). (For interpretation of the references to colour in this figure legend, the reader is referred to the web version of this article.)

up to 25–35% when 4 mol.% H₂O (1–1.5 wt% of H₂O; see section 6.1.3) is added to the system. The P-T range of this field where Bt, Crd, Sil and melt coexist is independent of the H₂O and redox variations. These data suggest the need for an external H₂O flux to generate diatexites (>25–30% melt) from the studied composition at the investigated P-T conditions.

6.1.2. Composition and A-X model considerations: garnet, cordierite and biotite

Garnet stability can be influenced by minor variations in the MnO composition (White et al., 2014b), which could be due in part to analytical uncertainty. Therefore, to check this influence on the

calculation results, we have recalculated the Grt-in (Grt-in) curve with less than half of the measured MnO content (0.03 mol%) in Thermocalc (Fig. 10), as presented in Section 4.4. The control calculation shows an increase of pressure of approximately 0.01–0.1 GPa compared to the previous Grt-in curve.

Regarding Crd and Bt, we have used the previous thermodynamic database (ds55; Holland and Powell, 1998), the hCrd A-X model for Crd (Perple_X ideal mixing model) and the Bio(TCC) A-X model for Bt (Tajčmanová et al., 2009) to check the influence of other models on the stability curves for these minerals. The calculated stability curves (Perple_X. 6.8.9) for these two phases are displaced towards higher temperature, by 10–20 °C for Crd and by 20–25 °C for Bt (Fig. 10). This affects the P-T region where the

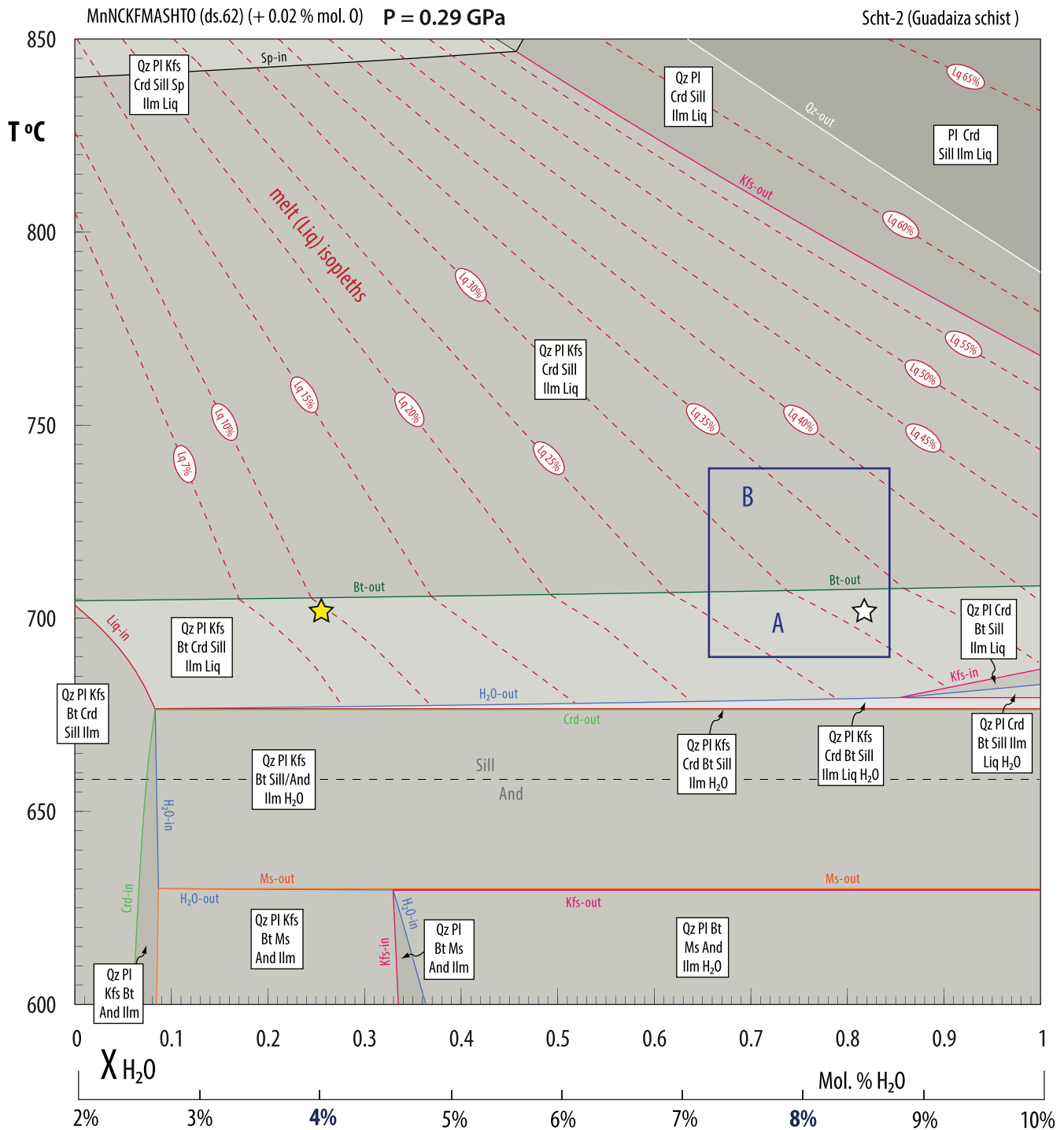


Fig. 11. T-X (H₂O) pseudosection of the Guadaiza schist (sample scht-2). Calculated modal melt isopleths are shown in red dashed lines (Liq = Lq). Yellow star indicates the same as in the P-T pseudosection. White star shows the following modal assemblage coexisting with 30–32% of melt (Liq): Qz (13%) + Kfs (10%) + Pl (8%) + Crd (25%) + Bt (5%) + Sil (6%) + Ilm (1%). The blue square with case A indicates an addition of +4 mol.% H₂O (1–1.15 wt%) to the initial conditions (yellow star) increasing the melt up to 25–35%. Case B also simulates the addition of +4 mol.% H₂O but with 20–30 °C heating and Bt overstepping, generating 30–40% of melt. Mineral/phase abbreviations according to Whitney and Evans (2010). (For interpretation of the references to colour in this figure legend, the reader is referred to the web version of this article.)

migmatite target assemblage occurs (Bt + Crd + Sil), displacing it up to T ≤ 740 °C (at the same pressures) and increasing the melt fraction to 11–15%.

We conclude that, even with the use of previous thermodynamic database models, the calculated melt proportion is far below that of necessary to form the observed diatexites in the Guadaiza unit, which require more than 25–30% melting.

6.1.3. T-X pseudosection

Fixing the pressure at 0.29 GPa, a T-XH₂O pseudosection of the Guadaiza schists was constructed in order to calculate the water content necessary to reach the melting degree inferred for the diatexites (melt % >25–30%) in the P-T field with Bt + Crd + Sil (Fig. 10). In the calculations, the water content was varied from 2 to 10 mol.%. The calculated diagram shows that water saturation

is reached at 2.6–2.7 mol.% of H₂O at this pressure (Fig. 11), therefore the 4 mol.% H₂O indicated by the P-T pseudosection (Fig. 10) already results in water-oversaturation of the system. Undersaturation (H₂O < 2.6–2.7 mol.%) would stabilize Crd at lower temperatures, which is not observed in the studied rocks. By the addition of water, most of the field assemblages and boundaries remain unaffected, except those involving Kfs, which are reduced (Kfs-out lines appearing towards more H₂O-rich domains). This is due to the involvement of Kfs in the water present melting, together with Qz and Pl. As the melt fraction increases due to the increase in H₂O content, the melt proceeds exclusively by the reaction $Qz + Pl + Kfs + H_2O \rightarrow \text{melt}$. The box labeled A and B in the Fig. 11 represents the zone where the melt fraction reached values between 25–40 % while keeping the assemblage of Crd + Sil ± Bt stable. These conditions can be achieved by adding about 4 mol.% of H₂O (1–1.5 wt% H₂O) to the initial H₂O (4 mol.%). At this point, two possibilities can be considered. In the first case (Case A), H₂O is added to the system while the field assemblage of Bt + Crd + Sil (+Qz + Pl + Kfs + Ilm) remains the same. In this scenario, the melt fraction reaches approximately 25–35 % for temperatures of 700–705 °C. The modal fraction of Bt-Crd-Sil remains very similar to those calculated at 4 mol.% of H₂O. In the second case (Case B), H₂O influx is accompanied by heating and the system shifts above the Bt-out boundary. In this case, the melt could reach up to 30–40 %. Biotite may persist metastable if the heating was fast and the Bt-out reaction was slightly overstepped. The irregular morphologies observed in the Bt that form part of restites in the heterogeneous granites agree with this latter process (Fig. 6E).

6.1.4. Composition of the melt, biotite and cordierite

The composition of the melt was calculated with Thermocalc for the P-T domain where the Guadaiza diatexites mineralogy and the calculated assemblage coincide (0.29–0.30 GPa, 700–705 °C). The calculated melt (9 %) coexisting with Bt + Crd + Sil has a peraluminous (A/CNK = 1.13) leucogranite composition with elevated K₂O/Na₂O (1.77) and very high FeO_t/FeO_t + MgO (0.98), typical of ferroan granites (Frost et al., 2001) (all values expressed as mass ratios except for A/CNK). The composition of Bt (ca. 5 modal%) and Crd (ca. 26 %) coexisting with this melt have FeO_t/(FeO_t + MgO) calculated values of 0.81 and 0.67, respectively.

These compositions are slightly different to those measured by XRF and EMPA in the studied rocks. The ASI mean value in the diatexites is 1.8 (range: 1.12–2.39), K₂O/Na₂O is 1.6 (range: 0.12–2.3) and FeO_t/FeO_t + MgO is 0.77 (range: 0.53–0.83). Regarding mineral compositions, the measured FeO_t/FeO_t + MgO average is 0.78 for Bt (n = 6) and 0.70 for Crd (n = 3) (Supplementary Material 2).

These differences are of some importance in the case of the Fe/Fe + Mg ratios, both in the bulk rock and mineral compositions. Adding H₂O to the system decreases this ratio in the melt (0.91), although it is still higher than those observed in the studied rocks. These discrepancies might indicate that the source rock for the diatexites could have had less FeO_t/FeO_t + MgO bulk ratios than the one selected for the pseudosections. Such compositional variations are common in metapelites/metagreywackes (Forshaw and Pattison, 2022) and can occur in the studied regional schist sequences.

6.2. P-T conditions of the Guadaiza unit compared to that of the Jubrique unit

We calculated P-T conditions of the Jubrique unit based on the Grt-bearing gneiss (sample Ju7 from Barich et al., 2014), which is lithologically similar to Jubrique gneisses studied previously in the literature (e.g., Barich et al., 2014; Massonne, 2014; Acosta-Vigil et al., 2016). The calculations were carried out using the new thermodynamic data set (ds62; see Methods), and its

correspondent mineral A-X models. The results indicate slightly lower pressures and temperatures for the previously recognized melting events (Supplementary Material 5). Nevertheless, the general P-T pseudosection topology is equivalent to the published results (mentioned above: section 2.3), and situates the higher-pressure melting event at 0.90–1.05 GPa and 770–800 °C, and the lower-pressure one at 0.42–0.48 GPa and 710–765 °C. The calculated melt degree in these two cases is, however, strikingly different. The high-pressure event indicates about 13 % melt fraction, in contrast to 2–3 % in the lower pressure zone.

The P-T estimation in the Guadaiza unit was accomplished based on the sample Scht-2 (Fig. 10) and the heterogeneous granite GH-1 (Supplementary Material 6). Comparing the results of calculations in the Jubrique and Guadaiza units, we observe that the higher-pressure melting is not recorded in the Guadaiza unit, while the lower pressure one took place at slightly deeper levels in the Jubrique (0.42–0.48 GPa and 710–765 °C) than in the Guadaiza unit (0.25–0.36 GPa and 675–710 °C). Moreover, the melting of Jubrique crust is consistent with the stability of Grt, as predicted by thermodynamic models too, while this phase is not stable and was not observed in the Guadaiza-type crust during the lower pressure melting event. Finally, the calculated melt fractions also differ, as during the lower pressure event the Jubrique crust was less productive (2–3 % melt) compared to the Guadaiza unit (6–11 % melt).

7. Geochronological results

7.1. Sample description

Three samples of migmatitic rocks were selected for this study. Sample OJ-02 represents the lower part of the Ojén unit, which can be observed in the southeast corner of the Fig. 2. Similarly to Guadaiza-type crustal section, diatexites and metatexites are found atop of Spl ± Pl peridotites, but overlain by a thick sequence of carbonatic rocks (Sierra Blanca). Metatexites are characterized by a compositional layering with leucocratic Qz + Kfs + Pl and mesocratic Bt + Crd + Sil bands. Garnet is scarce or absent in these rocks. There are abundant leucosome-filled shear zones and intrafoliation folds. The Istán orthogneiss is represented by sample Gn1st-1. As documented above, together with associated leucogranites, these rocks show an equivalent position in Guadaiza-type crustal sequences to the heterogeneous granites. The orthogneisses consist of Kfs porphyroclasts contained in a highly strained matrix with Qz + Kfs + Pl + Bt + Sil + And ± Grt as major constituents. The MA-05 migmatites were sampled south of Benahavís, in a roughly E-W orientation of ductile–brittle structures characterized by highly serpentinized peridotites overthrusting crustal units. These migmatites present Bt + Grt + Sil rich mesosomes cut by thick leucogranitic bodies with abundant Grt. They are similar to Jubrique-type migmatites.

In addition, we analyzed four samples of heterogeneous granites in different locations in the study area, always in contact with Spl ± Pl peridotites. MA-07 and SN-18 diatexites were collected far from the main structures of the study area. SN-18 granites form a small body surrounded by ultramafic rocks, and MA-07 represents the base of a more complete Guadaiza-type crustal sequence, with metatexites and schists above, south of the Guadaiza valley. They show little or no ductile deformation and are composed of a medium-grained matrix of Qz + Pl + Kfs and scarce Bt, large crystals of Crd, Pl, Kfs and occasionally Tur, and Bt + Crd + Sil ± And restites. On the contrary, SN-62 and SN-67 show intense ductile deformation. These are mylonitic granites sampled north and south of the NNW-SSE shear zone that crosses the study area between Sierra de las Nieves and Montemayor (Fig. 2). They are compositionally similar to other heterogeneous granites, although they present a

ages, but undeformed heterogeneous granites SN-18 and MA-07 reached up to 95 % of pre-Permian ages after more than 50 analyses per sample. Neoproterozoic ages are the most represented among the inherited ages, although these results are not meaningful for estimating provenances or maximum depositional ages.

Sample by sample, zircon populations and analytical results are as follows (Fig. 12, Supplementary Material 3 and 4). Zircons from the Grt-rich migmatites near Benahavís (MA-05) show euhedral to subhedral, medium- to coarse-grained crystals composed of a highly altered inner zone and an extensive external overgrowth with low luminosity in CL images. This zircon sample also contains a minor amount of small, simple crystals. Analytical results ($N = 33$), carried out in unaltered areas, yield an important group of Permian ages ($N = 14$; 284–258 Ma) and two secondary groups with Triassic and Miocene ages ($N = 7$ and 9, respectively). Permo-Triassic ages were analyzed in larger, dark external overgrowths surrounding metamictic areas. Miocene ages were found in thinner external areas grown over these altered zones and in simple, small zircons (Fig. 12). All analyses show high U contents (>3000 ppm) and Th/U mass ratios lower than 0.01.

The Istán orthogneiss (sample Gnlst-1) presents a complex zircon population composed of fragments of large, simple crystals and compound zircon grains constituted by rounded cores with parallel banded or concentric structure, many of them with high luminosity in CL, and an external overgrowth with concentric or faint zonation. Similar to the Jubrique-type migmatite (sample MA-05), zircons from the Istán orthogneiss are highly affected by alteration in different crystal areas, as documented in previous studies (Acosta-Vigil et al., 2014). After 30 analyses, in addition to inherited ages (pre-Permian ages, 40 %), nine spots yielded Permian ages (285–254 Ma) and other nine analyses gave younger data dispersed between the Triassic and Eocene. Analyses providing Permo-Triassic ages present Th/U ratios ranging between 0.7 and 0.01 and low U contents. On the contrary, younger ages resulted from analyses with U contents above 2000 ppm and Th/U < 0.01 (Supplementary Material 3).

Zircons from the Ojén metatexites (OJ-02) also show a great variety of forms and inner structures, as expected for migmatitic rocks. They are mostly stubby or short prisms composed of core and external overgrowth. After 51 analyses, the results are clearly clustered around Permian ages (almost 50 % of all data) and analyzed in well-developed concentric overgrowths (Fig. 12). Again, younger ages are scattered between Triassic and Miocene, highlighted by four analyses that yielded 21 Ma, analyzed in external dark rims with faint zonation. U contents are lower than 3000 ppm, although Th/U mass ratios are mostly below 0.01, with higher values in Permian ages.

Mylonitic heterogeneous granites SN-62 and SN-67 present mostly rounded, anhedral, small- to medium-grained crystals dominated by a large inherited core surrounded by thin external overgrowths. In detail, zircon populations of mylonitic heterogeneous granites include small, unzoned or parallel banded simple grains and complex zircons composed of an inherited core and a variety of rims, e.g., concentric or faint zonation, dark or high luminosity in CL, inward overgrowths typical of granulitic rocks (Corfu et al., 2003). Even though analyses are focused on these external areas of zircon grains (spots are systematically located in thin overgrowths), more than 50 % of the analyses yielded pre-Permian ages, considered inherited, after 130 analyses. Both samples present a minor number of Permian ages, and a significative group of Miocene ages, mainly analyzed in very thin external rims, constituted by mostly concordant ages between 22 and 20 Ma and younger analyses with high common Pb contents and discordance (Supplementary Material 3). In addition, Mesozoic and Paleogene ages are dispersed between the above-mentioned groups. In general, U contents are variable and Th/U mass ratios are lower than 0.01.

Undeformed heterogeneous granites SN-18 and MA-07 present similar zircon crystals to those in mylonitic ones (i.e., SN-62 and SN-67). Complex crystals characterized by large inherited cores dominate zircon populations with a few simple acicular grains (Fig. 12). Similarly, despite the significant number of analyses per sample, post-Carboniferous ages only represent 10 %, with distinct Permian ages and a set of dispersed younger results.

Considering the similarities in geochronological results and zircon populations of migmatites, gneisses, as well as mylonitic and undeformed heterogeneous granites, below we present the characteristic post-Carboniferous age clusters. All analyzed samples show Permian ages, which are predominant in the migmatites. These are mostly concordant data (Fig. 13A), accumulating 50 % of the probability of all analyses, excluding the inherited ages (Fig. 13B). Permian ages are widely distributed between 290 and 254 Ma, although many are clustered around a maximum peak of 272 Ma (Fig. 13B). On average, these results show low discordance percentages and low common Pb values, moderate U contents, and a mean Th/U mass ratio of 0.08. Ages between 240 and 220 Ma are not easily distinguished from the Permian results and are present throughout all groups of samples. However, analyses yielding ages younger than 240 Ma show increasing discordance and higher common Pb values and contain the highest U concentrations. Besides, Mesozoic and Paleogene results are likely randomly distributed without discernible mean ages, and altogether they comprise a negligible probability percentage in the geochronological database (<15 %; Fig. 13). The youngest age group is early Miocene, accounting for roughly 25 % of post-Carboniferous ages. This group, however, is only present in thin, external overgrowths of zircons in migmatites (OJ-02 and MA-05) and in the mylonitic heterogeneous granites (SN-62 and SN-67), whereas it has not been detected either in the Istán orthogneiss (Gnlst-1), or in the undeformed heterogeneous granites (MA-07 and SN-18). Although statistical values of Miocene ages show high discordance and high common Pb values, those ranging between 22 and 20 Ma are mostly concordant averaging around 21 Ma, which is a well-known, characteristic age in the Betic Cordillera (Fig. 13).

8. Discussion

8.1. Nature of the contacts between crustal and mantle units

Regarding the structural position of the Ronda peridotites in relation to the crustal units, the results presented here contradict the prevailing view that the peridotites overlie the Guadaiza unit by a basal thrust (e.g., Lundeen, 1978; Torres-Roldán, 1983; Tubía and Cuevas, 1986; Tubía et al., 1997, 2013; Esteban et al., 2008), and are underlain by the Jubrique unit, separated from the metamorphic envelope by a ductile shear zone (e.g., Balanyá et al., 1993; Tubía et al., 1997; Argles et al., 1999; Platt et al., 2003a). These lower and upper contacts of the peridotites and the associated partial melting are generally explained as dynamothermal aureoles formed in Alpine times. In this scenario, the lower contact with the Guadaiza-type units represents hot thrusting during intracrustal emplacement of mantle rocks, and the upper contact with the Jubrique-type units represents syn- to late-orogenic extensional unroofing (e.g., Argles et al., 1999; Frasca et al., 2017; Gueydan et al., 2019; Hidas et al., 2013a; Homonnay et al., 2018; Mazzoli and Martín-Algarra, 2011; Platt et al., 2003a,b, 2013; Tubía et al., 1997; Tubía and Cuevas, 1986).

Field relations reveals that the Guadaiza crustal unit lies atop the P1 tectonite domain of the Ronda massif (Fig. 5). Geochemical and thermobarometric results suggest that Guadaiza mid-crust schists, which preserve relict Grt and pre-kinematic And, were juxtaposed to mantle rocks during continental rifting. During this

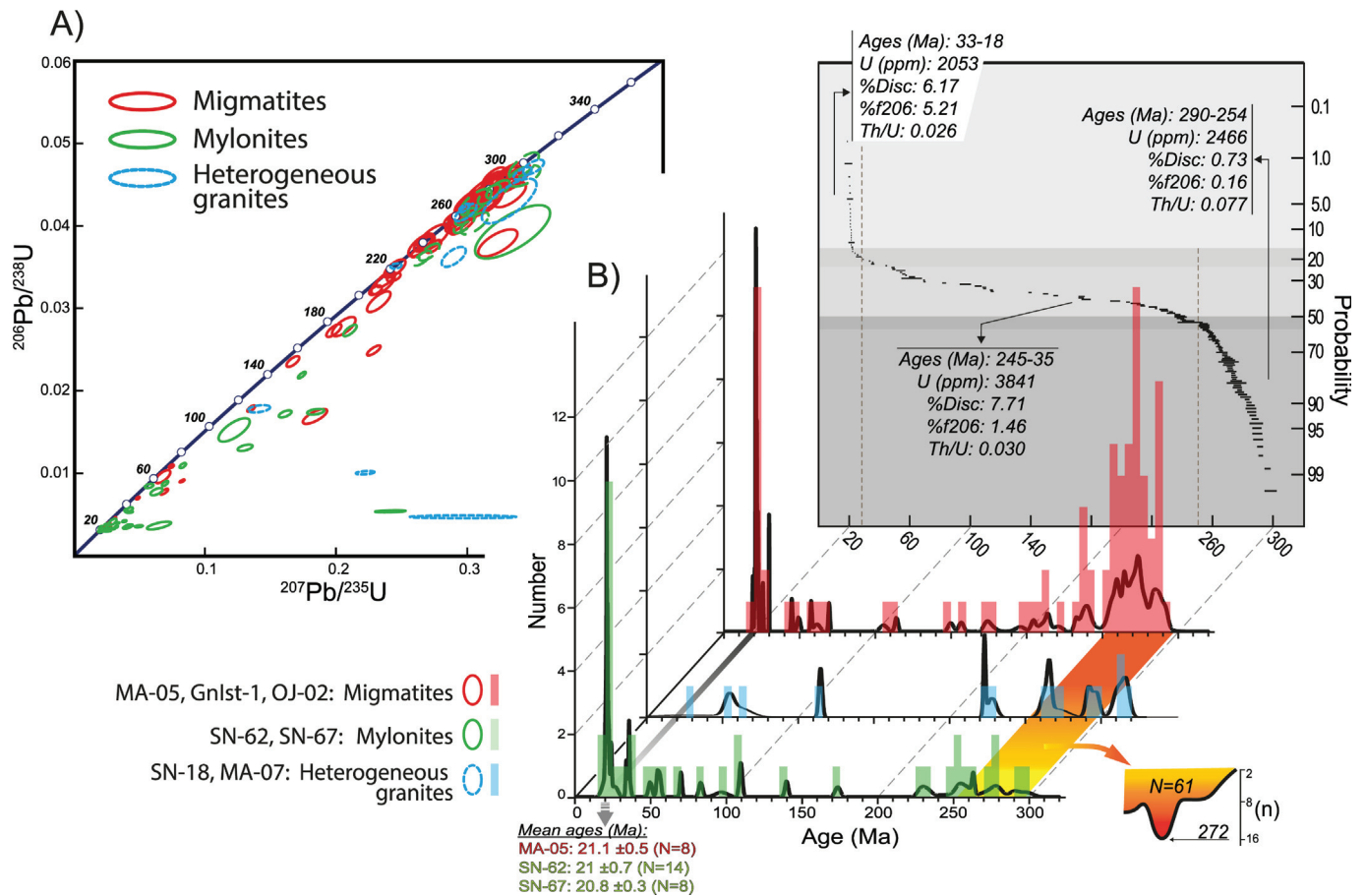


Fig. 13. A) Concordia diagram showing U-Pb uncorrected isotopic ratios of the studied samples (Supplementary Material 3). Error ellipses represent a 2σ conf., including the standard error. B) Relative probability histogram and probability plot showing the distribution of ages resulted in the geochronological study. The histogram presents the main groups of samples: migmatites (MA-05, Gnlst-1 and OJ-02), mylonitic heterogeneous granites (SN-62 and SN-67) and undeformed heterogeneous granites (SN-18 and MA-07). However, all data were included in the estimation of cumulative probability and statistical parameters (geochronological uncertainties), separating Permian, Triassic to Eocene and late Oligocene to early Miocene results.

process of crustal attenuation, metasedimentary protoliths underwent low-pressure partial melting to finally constitute the migmatitic basal unit of the Guadaiza-type crust (Figs. 7–10). The total loss of pre-rift lower crust in these sectors is suggested by this arrangement of mid-crustal units in direct contact with the mantle. While both the crustal and ultramafic rocks exhibit pronounced high-temperature tectonic foliation, it is important to note that there is no discrete shear zone with increasing strain toward the petrologic Moho in contact with the Guadaiza unit. Rather than subsolidus strain localization, the mid-crust exhibits partial melting and ductile deformation pattern of variable intensity as a result of flattening, which is suggested by the oblate mesoscopic shape of restites, Qz resisters, and Kfs nodules (Fig. 6B and C). At that time, the peridotites developed a pervasive high-T tectonic foliation coeval with or subsequent to the subsolidus reaction of Spl to form Pl (Fig. 6F and G).

The basal part of the Jubrique lithospheric unit, from bottom to top, is composed of the Spl tectonites and Grt-Spl mylonites of the Ronda Peridotites, and the Grt gneisses of the crustal envelope, which is particularly well exposed in the northern part of Sierra Bermeja, and in two outcrops in the southern part of our study area, near Montemayor and the Concepción reservoir (Fig. 2). The Grt-Spl domain is interpreted to have been originally deeper than the Spl domain, consistent with Garrido et al. (2011). As we have noted, the extensional deformation recorded by both domains was coeval and, in contrast to the Guadaiza unit, with increasing strain toward the contact with the crustal rocks.

High-angle reverse and reverse-oblique faults locally juxtaposed mantle over crustal domains during Aquitanian times, i.e. during the inversion of the rifted margin. They facilitate melt/fluid percolation at different levels in the lithosphere. These structures play a key role in both the crustal anatexis and peridotite serpentinization at shallow depths by facilitating fluid/melt migration, and their reactivation in the Alpine orogenesis is the reason that potentially led to controversial structural models of peridotite emplacement.

8.2. Implication of absolute ages

The geochronological study carried out on migmatites and heterogeneous granites of the study area, in contact with the Ronda Peridotites, is intended to obtain the age of the partial melting and metamorphic processes that established the lower parts of the Jubrique and Guadaiza crustal units atop of their coupled ultramafic facies. Textural, morphological, and chronological evidence suggest that the studied zircon populations are constituted by a few zircons crystallized directly from anatexitic melts, zircons removed from mesosomes, and inherited zircons from the sedimentary protoliths overgrown in granitic melts or during later metamorphic processes. Actually, despite the significant melting percentage inferred for the formation of metatextitic migmatites and heterogeneous granites (diatexitic migmatites) (Figs. 10 and 11), simple, acicular zircons crystallized directly from partial melts are scarce (Fig. 12; Supplementary Material 3 and 4). Although

aimed at provenance analysis of crustal units, thus focused on detrital zircon populations, earlier geochronological studies carried out in metamorphic rocks of the study area provided a large group of pre-Permian ages, as well as a few Permo-Triassic and a negligible number of Miocene analyses (Esteban et al., 2011b, 2022).

The high percentage of zircon inheritance observed in lower crustal units of the western Betics points to notable inferences about the melting process. A first-order constraint for zircon dissolution and crystallization is the silicic, highly peraluminous compositions of partial melts derived from Guadaiza schists (Fig. 7). These anatectic melts (“cold granites” in the sense of Miller et al., 2003) require fluid influx and are rapidly saturated in Zr, restricting zircon dissolution from the source (Watson and Harrison, 1983; Miller et al., 2003). Secondary causes invoked for this anomalously high inheritance are a fast-melting event and the presence of restitic Bt that may shield zircon grains and prevent dissolution. A similar water-present and fast melting event (overstepped Bt-out reaction) (Fig. 11) is deduced from the need to increase the melting percentages to produce diatexites (heterogeneous granites).

Regarding post-Carboniferous data, all samples yield Permian ages, constituting a well-defined cluster of concordant ages with low common Pb. Altogether, Permian ages represent 50 % of the probability and represent the largest amount of non-inherited ages in migmatites and unstrained heterogeneous granites. They show low Th/U mass ratios, between 0.3 and 0.01 (0.08 on average), although these ratios are higher than those obtained in younger analyses, closer to or even lower than 0.01 (Fig. 13). These data suggest that Permian simple zircons and zircon overgrowths were crystallized during prograde metamorphism and from a felsic peraluminous melt (e.g., Williams and Claesson, 1987; Pereira et al., 2014). The Permian cluster shows $^{206}\text{Pb}/^{238}\text{U}$ ages distributed between 290 and 255 Ma, even showing a somewhat indistinct trend towards Triassic ages. However, a notable amount of data points to an age of 272 Ma as the best estimation of this metamorphic/partial melting event (Fig. 13).

Geochronological results highlight another relevant age during the evolution of the western Betics around 21 Ma. Early Miocene ages are dominant among post-Carboniferous data in mylonitic heterogeneous granites (SN-62 and SN-67) and show variable percentages in migmatites (27 % in Grt-migmatites MA-05 but only four analyses in sample OJ-02) (Fig. 12). However, they are absent in undeformed heterogeneous granites and Istán gneisses. Although the youngest analyses are scattered between 25 and 15 Ma, only results around 21 Ma show low discordance and common Pb (Fig. 13). Early Miocene ages were analyzed in thin external overgrowths with the lowest Th/U ratios (0.02 on average), typical of metamorphic recrystallization. Ages between 23 and 18 Ma (only low discordance data) yield the same age within analytical uncertainty, giving an accurate weighted mean $^{206}\text{Pb}/^{238}\text{U}$ age of 21 Ma (N = 30 adding samples SN-62, SN-67 and MA-05) (Fig. 13).

The location of samples with early Miocene ages may shed light on the tectono-metamorphic evolution of lower crustal rocks and the age of metamorphic events. Thus, samples that yielded a significant Miocene recrystallization are located in primary structural lineaments, i.e., the NNW-SSE mylonitic shear zone that put into contact with the Guadaiza and Jubrique units (SN-62 and SN-67) and the brittle-ductile structures that stack crustal metamorphic rocks and highly serpentinized peridotites to the south of the study area (MA-05). We suggest that the same thermal reactivation that promoted zircon recrystallization close to regional structures may have produced metamictic processes and isotopic disequilibrium in previously crystallized zircons (Permian), leaving a trail of discordant, meaningless ages between Permo-Triassic and Miocene,

in agreement with previous geochronological studies carried out in the Guadaiza unit (Acosta-Vigil et al., 2014). Merely the proximity to mantle rocks and the thermal influence of the dynamothermal aureole, as proposed by previous authors (e.g., Lundeen, 1978; Torres-Roldán, 1983; Tubía and Cuevas, 1986; Tubía et al., 1997, 2013; Esteban et al., 2008), cannot account for the presence of Miocene ages, because in this study all the samples are in contact with peridotites of the same tectono-metamorphic facies, while only the ones located along large-scale tectonic structures record these ages. Additionally, our results also indicate that the Miocene age of leucogranites in the study area (e.g., Esteban et al., 2011a, and references therein) might only represent a shallow magmatic event associated with the contractional reactivation of pre-existing extensional structures, thus these ages cannot be directly linked to the intracrustal emplacement of the Ronda Peridotites.

Therefore, we propose that an extended low-pressure and medium- to high-temperature metamorphism and partial melting occurred in the lower crust of the Guadaiza unit, generating metatexites and diatexites with limited zircon dissolution and recrystallization, which was controlled mainly by the composition of the melt. A similar late Variscan evolution has been depicted by Lu-Hf ages in granoblastic Grt gneisses of the Jubrique unit (Barich, 2015), or by U-Pb ages in monazites studied in Ky-bearing graphitic metapelites to the east of the study area (Sánchez-Navas et al., 2024). Subsequently, the Alpine orogenic reactivation, which probably nucleated along previous extensional structures, triggered a thermal input that promoted zircon recrystallization limited to those rocks located along structural lineaments but affecting the isotopic ratios of Permian zircons in the entire study area. The 21 Ma zircon recrystallization may be associated with the tectonic stacking, shear heating, the infilling of hydrothermal fluids, also related to the serpentinization of peridotites along these structures, or, to a lesser extent, to the intrusion of volumetrically poor, leucogranitic dikes.

8.3. Pre-orogenic kinematic evolution

The proposed kinematic model incorporates two superimposed rifting events that ultimately result in hyperextension and oceanic spreading (Fig. 14). The temperature and pressure conditions prior to rifting were calculated to be approximately 0.90–1.05 GPa and 770–800 °C in the lower crust (e.g., Barich, 2015), and roughly 2.7 GPa/1100 °C in the lower portion of the mantle lithosphere (e.g., Garrido et al., 2011) (Fig. 14A). During the first Permian-Triassic rifting stage, the upwelling of the asthenosphere probably counterbalanced the rapid thinning of the lithospheric mantle. The mantle underwent significant attenuation and uplift beneath two major conjugate shear zones (black arrows in Fig. 14B and C). In these shear zones and along the crust-mantle interface, the lower crust and lithospheric mantle experienced simple shearing and mylonite formation, resulting in the incorporation of Grt-Spl-bearing relict peridotites near crustal levels (Fig. 14B and C).

A thermal anomaly linked to the asthenosphere upwelling took place across the most extended area. Under high temperature conditions, the weak strength of the lower crust marked the style of crustal extension resulting in partial melting within the lower crust coeval to decompression, ductile condensation and even partial removal of the lowermost crustal layer, and brittle-ductile attenuation of the upper crustal levels (Fig. 14C). Therefore, necking of the lower crust led to the placement of the pre-rift middle crust directly atop the lithospheric mantle also experiencing vertical flattening (cf. crust-mantle contact above the solid yellow line in Fig. 14C). This low-pressure, high- to medium-temperature event – 675–710 °C at ca. 0.3 GPa (Fig. 10) – produced important zircon recrystallization between 290 and 255 Ma. Altogether, the

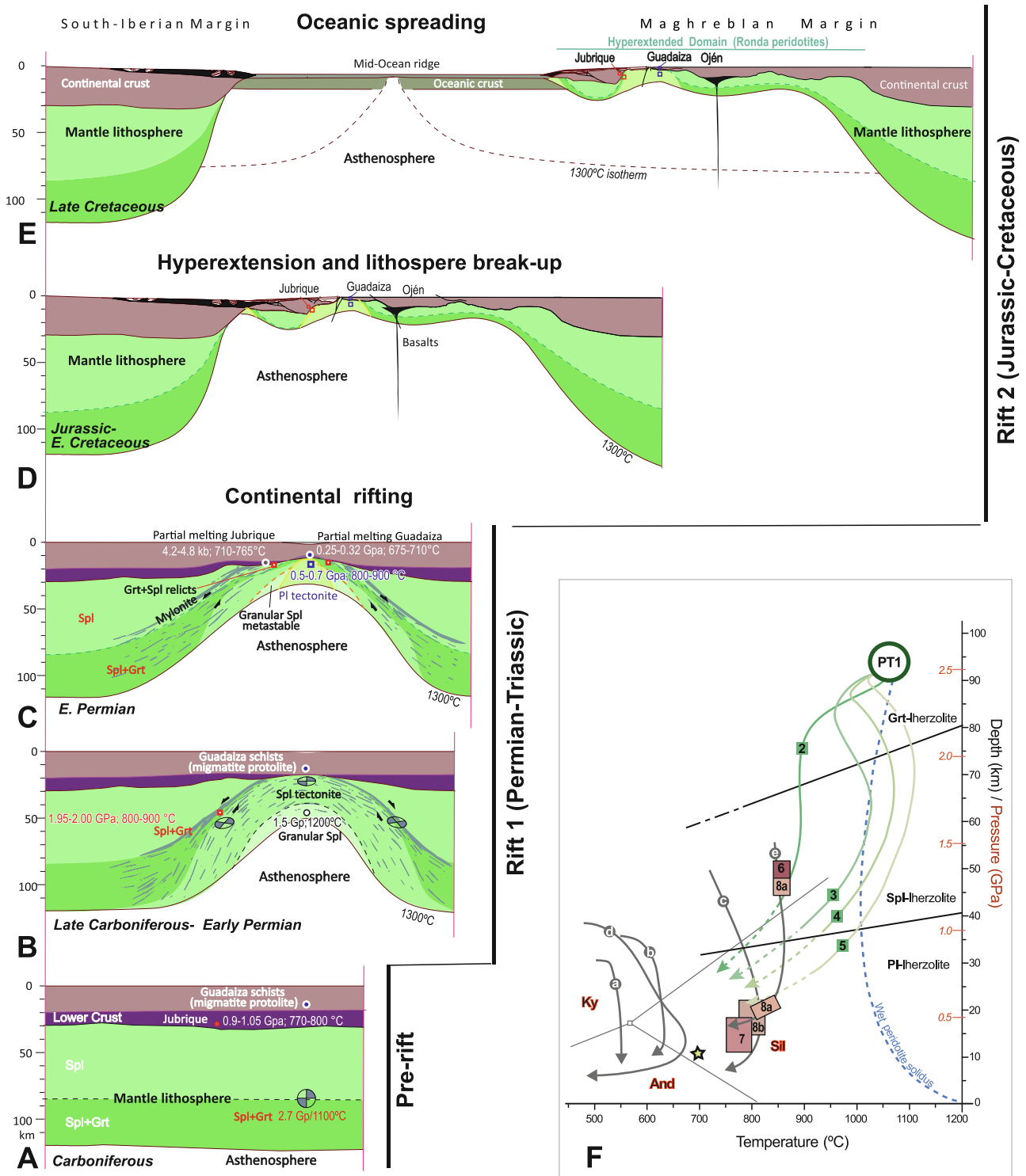


Fig. 14. Proposed kinematic evolution showing the tectono-metamorphic interaction of upper mantle peridotites and lower crustal units during (A-C) two superimposed rifting events, (D) hyperextension and (E) lithosphere break-up and oceanic spreading. F) P-T diagram summarizing the thermobarometric results obtained in this work and collected from the literature, depicting the Permo-Triassic, pre-Alpine evolution of crustal and mantle rocks in western Betic Cordillera. P-T trajectories of mantle facies: PT-1 – Initial conditions of Grt-Iherzolites (Garrido et al., 2011); 2–5 – P-T evolution estimated for the peridotite facies that constitute the Ronda massif, i.e.: Spl ± Grt mylonites (2), Spl tectonites (3), granular/transitional peridotites (4) and Pl tectonites (5) (after Johannesen et al., 2014). P-T trajectories of crustal units: Star – Heterogeneous granites (this work); (a-c) – crustal envelope of the Carratraca peridotitic massif (Argles et al., 1999); (d) – ODP-976 borehole in the Alborán sea (Soto and Platt, 1999); (e) – Kinzigites and Grt-migmatites of the Jubrique unit (Barich, 2015); (f) – Pelitic gneisses at the basement of the Torrox Unit (Upper Alpujarride) (Sánchez-Navas et al., 2024); (6) – Jubrique kinzigites (Barich et al., 2014); (7) – Guadiza heterogeneous granites (Acosta-Vigil et al., 2014); (8a) – Jubrique Grt-migmatites (Barich et al., 2014); (8b) – Guadiza migmatites (Acosta-Vigil et al., 2014).

revised structural position of crustal and mantle units, the thermodynamic modelling of the Guadaiza unit, and the new geochronological data unveil that the continental crust of Pangea had already undergone thinning to approximately 10 km thickness in certain areas by the end of the Permian. These P-T conditions are compatible with those inferred for the low-pressure, Pl-bearing peridotites, and allow for hypothesizing that mid-crustal schists were tectonically juxtaposed with mantle rocks through the petrologic Moho accompanied by a potentially fast, water-present melting process at the base of the Guadaiza-type crust (Fig. 14C). Meanwhile, the lithospheric mantle experienced moderate melting, as recorded by the formation of various types of pyroxenites mostly in the Spl- and Pl-bearing peridotites (e.g., Garrido and Bodinier, 1999; Bodinier et al., 2008), and re-equilibrated through Spl into Pl lherzolite facies (e.g., Obata, 1980). The origin of 1–1.5 wt% H₂O-fluids (4 mol.%; Fig. 11) necessary to increase melting percentages and generate the observed diatexites in the Guadaiza unit could have been channeled through a shear zone affecting both the crustal units and the shallowermost peridotites.

We propose that an additional rift phase during the Jurassic and Early Cretaceous resulted in hyperextension and final lithosphere break-up (Fig. 14D). Anastomosed brittle-ductile shear zones trending NNW-SSE and ESE-WNW cut the lithospheric mantle probably accommodating tens of kilometers of extension at that time. However, further studies are required to more precisely characterize the conditions and establish temporal constraints on the activity of these shear zones. Nevertheless, Jurassic and Early Cretaceous Lu-Hf Grt and U-Pb-Th zircon ages within Grt pyroxenites and chromitites reflect a thermal event linked to these extensional stages that preceded the oceanic spreading (e.g., Pedrera et al., 2021). In addition, volumetrically-poor basaltic magmatism, representing mantle-derived melts during subsequent Jurassic rifting stage (Fig. 14D), has been described in the Ojén unit (e.g., Tubía et al., 1997; Sánchez-Rodríguez and Gebauer, 2000). In contrast, there was no crustal melting during this Jurassic-Cretaceous rifting event. The final oceanic spreading is marked by the Late Cretaceous age of the deep-water sediment of the Campo de Gibraltar Complex, which are situated north and west of the studied area, presumably deposited over oceanic crust (Figs. 1 and 14E).

9. Conclusions

Cartographic and field relations, presented in new geological mapping and associated cross-sections, delineate two lithospheric units formed by the systematic tectonometamorphic association of crustal and mantle rocks, which suggests that the evolution of Guadaiza and Jubrique metamorphic units is closely related to their associated lithospheric mantle domain. These crustal sequences over the Ronda Peridotites form a lithosphere extremely attenuated during rifting. This genetic link between crustal and mantle units requires a reconsideration of the kinematic evolution of the massif before the onset of the contraction (Alpine orogeny), which is here associated with two superposed continental rifting events that ultimately resulted in the formation of the Maghrebian magma-poor hyperextended margin and oceanic spreading. The results presented here are in accordance with recent studies in the Beni Bousera mantle rocks which conclude that they were exhumed to a shallow depth during Triassic-Lower Jurassic rifting. The revised interpretation provides a correlation between the PT evolution of the crustal sequence, taking also into account partial melting events, and that of the tectono-metamorphic domains of the peridotites. Partial melting and the loss of the lower crust put forward the importance of Permian-Triassic rifting in the Betic realm, associated with HT-LP metamorphism in Permian times, in

accordance with the metamorphic conditions documented in the European Alps and Pyrenees.

New field, cartographic, thermobarometric, and geochronological evidence allows us to present the pre-Alpine evolution of the western Betics in a way that reconciles a large amount of data that has been collected in the cordillera in recent decades and links this western Mediterranean sector with the pre-Alpine evolution of the European Alps and Pyrenees. In all these sectors peripheral to the Mediterranean, the Permian hot rifting stage was precursor of subsequent mantle exhumation during Mesozoic.

CRedit authorship contribution statement

Juan Díaz-Alvarado: Conceptualization, Investigation, Methodology, Visualization, Writing – original draft, Writing – review & editing. **Luis González-Menéndez:** Investigation, Methodology, Visualization, Writing – original draft, Writing – review & editing. **Károly Hidas:** Conceptualization, Funding acquisition, Investigation, Methodology, Project administration, Writing – original draft. **Antonio Azor:** Conceptualization, Investigation, Validation, Writing – review & editing. **Antonio Pedrera:** Conceptualization, Investigation, Validation, Writing – review & editing.

Declaration of competing interest

The authors declare that they have no known competing financial interests or personal relationships that could have appeared to influence the work reported in this paper.

Acknowledgments

This is a work by the Tectonic Processes and GeoResources Lab (IGME-CSIC) supported by the project by the MCIN/AEI/10.13039/501100011033/. FEDER 'Una manera de hacer Europa' (REVisE-Betics-PID2020-119651RB-I00). We thank Jan Marten Huizenga, Associate Editor of Gondwana Research, and two anonymous reviewers for their detailed comments, which have significantly improved the manuscript. We also appreciate the valuable comments from Dr. Pilar Montero regarding the geochronological results. This is the IBERSIMS publication no 109.

Appendix A. Supplementary data

Supplementary data to this article can be found online at <https://doi.org/10.1016/j.gr.2024.03.018>.

References

- Acosta-Vigil, A., 1998. Estudio de los fenómenos de fusión cortical y generación de granitoides asociados a las peridotitas de Ronda. Universidad de Granada, Granada, Spain. Ph.D. thesis.
- Acosta-Vigil, A., Pereira, M.D., Shaw, D.M., London, D., 2001. Contrasting behaviour of boron during crustal anatexis. *Lithos* 56, 15–31.
- Acosta-Vigil, A., Rubatto, D., Bartoli, O., Cesare, B., Meli, S., Pedrera, A., Azor, A., Tajčmanová, L., 2014. Age of anatexis in the crustal footwall of the Ronda peridotites, S Spain. *Lithos* 210–211, 147–167.
- Acosta-Vigil, A., Barich, A., Bartoli, O., Garrido, C.J., Cesare, B., Remusat, L., Poli, S., Raepsaet, C., 2016. The composition of nanogranitoids in migmatites overlying the Ronda peridotites (Betic Cordillera, S Spain): the anatectic history of a polymetamorphic basement. *Contrib. Mineral. Petrol.* 171, 24.
- Altherr, R., Holl, A., Hegner, E., Langer, C., Kreuzer, H., 2000. High-potassium, calc-alkaline I-type plutonism in the European Variscides: Northern Vosges (France) and northern Schwarzwald (Germany). *Lithos* 50 (1–3), 51–73.
- Andrieux, J., Fontboté, J.M., Mattauer, M., 1971. Sur un modèle explicatif de l'Arc de Gibraltar. *Earth Planet. Sci. Lett.* 12, 191–198.
- Argles, T.W., Platt, J.P., Waters, D.J., 1999. Attenuation and excision of a crustal section during extensional exhumation: The Carratraca Massif, Betic Cordillera, southern Spain. *J. Geol. Soc. London* 156, 149–162.
- Azañón, J.M., Balanyá, J.C., García-Dueñas, V., 1995. Registro metamórfico de alta presión-baja temperatura en la unidad de Jubrique e imbricaciones de Benarrabá (Cordillera Bético-Rifeña). *Geoceta* 17, 133–134.

- Baedecker, P.A., 1987. Methods for geological analysis. U.S. Geol. Surv. Bull., p. 1770.
- Balanyá, J.C., Azañón, J.M., Sánchez Gómez, M., García Dueñas, V., 1993. Pervasive ductile extension, isothermal decompression and thinning of the Jubrique unit in the Oligocene (Alpujarride Complex, Western Betics Spain). *C. r. Acad. Sci. Ser. II* 316, 1595–1601.
- Balanyá, J.C., García Dueñas, V., 1987. Structural Trends of the Alboran Domain on Both Sides of the Straits of Gibraltar. *C. r. Acad. Sci. Ser. II* 304, 929–933.
- Balanyá, J.C., García-Dueñas, V., 1991. Estructuración de los Mantos Alpujarrides al W de Málaga (Béticas, Andalucía). *Geogaceta* 9, 30–33.
- Balanyá, J.C., García-Dueñas, V., Azañón, J.M., Sánchez Gómez, M., 1997. Alternating contractional and extensional events in the Alpujarride Nappes of the Alboran domain (Betics, Gibraltar arc). *Tectonics* 16, 226–238.
- Barich, A., 2015. Unravelling the anatectic history of the lower continental crust through the petrology of melt inclusions and lu-hf garnet geochronology: A case study from the western Alpujarrides (Betic Cordillera, S. Thesis, Universidad de Granada, Spain), p. 200.
- Barich, A., Acosta-Vigil, A., Garrido, C.J., Cesare, B., Tajčmanová, L., Bartoli, O., 2014. Microstructures and petrology of melt inclusions in the anatectic sequences of Jubrique (Betic Cordillera, S. Spain): Implications for crustal anatexis. *Lithos* 206–207, 303–320.
- Bea, F., Montero, P., Stroh, A., Baasner, J., 1996. Microanalysis of minerals by an Excimer UV-LA-ICP-MS system. *Chem. Geol.* 133, 145–156.
- Bessière, E., Augier, R., Jolivet, L., Précigout, J., and Romagny, A., 2021. Exhumation of the Ronda peridotite during hyper-extension: New structural and thermal constraints from the Nieves Unit (Western Betic Cordillera, Spain). *Tectonics* 40, e2020TC006271. doi:10.1029/2020TC006271.
- Black, L.P., Kamo, S.L., Allen, C.M., Aleinikoff, J.N., Davis, D.W., Korsch, R.J., Foudoulis, C., 2003. TEMORA 1: a new zircon standard for Phanerozoic U-Pb geochronology. *Chem. Geol.* 200, 155–170.
- Blanco, M.J., Spakman, W., 1993. The P-Wave Velocity Structure of the Mantle Below the Iberian Peninsula - Evidence for Subducted Lithosphere Below Southern Spain. *Tectonophysics* 221, 13–34.
- Bodinier, J.L., Garrido, C.J., Chanefo, I., Bruguier, O., Gervilla, F., 2008. Origin of pyroxenite-peridotite veined mantle by refertilization reactions: Evidence from the Ronda peridotite (Southern Spain). *J. Petrol.* 49, 999–1025.
- Bouillin, J.P., Durand-Delga, M., Olivier, P., 1986. Betic-Rifian and Tyrrhenian Arcs: distinctive features, genesis, and development stages. In: Wezel, F.C. (Ed.), *The Origin of Arcs*. Elsevier Science Publishers, Amsterdam, pp. 281–304.
- Bouybaouene, M., Michard, A., Goffe, B., 1998. High-pressure granulites on top of the Beni Bousera peridotites, Rif belt, Morocco: a record of an ancient thickened crust in the Alboran domain. *Bull. Soc. Géol. France* 169, 153–162.
- Boynton, W.V., 1984. Cosmochemistry of the rare earth elements; meteorite studies. In: Henderson, P. (Ed.), *Rare Earth Element Geochemistry*. Elsevier Science Publishers B. V., Amsterdam, pp. 63–114.
- Brune, S., Heine, C., Perez-Gussinye, M., Sobolev, S.V., 2014. Rift migration explains continental margin asymmetry and crustal hyperextension. *Nat. Commun.* 5, 4014. <https://doi.org/10.1038/ncomms5014>.
- Brune, S., Kolawole, F., Olive, J.A., Stamps, D.S., Buck, W.R., Buitter, S.J.H., Furman, T., Shillington, D.J., 2023. Geodynamics of continental rift initiation and evolution. *Nat. Rev. Earth Environ.* 4, 235–253. <https://doi.org/10.1038/s43017-023-00391-3>.
- Casciello, E., Fernández, M., Vergés, J., Cesarano, M., Torne, M., 2015. The Alborán domain in the western Mediterranean evolution: the birth of a concept. *Bull. Soc. Géol. France* 186, 371–384.
- Castro, A., 2013. Tonalite-granodiorite suites as cotectic systems: a review of experimental studies with applications to granitoid petrogenesis. *Earth Sci. Rev.* 124, 68–95.
- Chamón-Cobos, C., Estévez González, C., Piles Mateo, E., 1978. In: *Mapa Geológico De España*, p. 37.
- Claoue-Long, J.C., Compston, W., Roberts, J., Fanning, C.M., 1995. Two Carboniferous ages: a comparison of SHRIMP zircon dating with conventional zircon ages and ⁴⁰Ar/³⁹Ar analysis. In: Berggren, W.A., Kent, D.V., Aubry, M.-P., Hardenbol, J. (Eds.), *Geochronology, Time Scales and Global Stratigraphic Correlation*, p. 362.
- Clerc, C., Ringenbach, J.-C., Jolivet, L., Ballard, J.-F., 2018. Rifted margins: Ductile deformation, boudinage, continentward-dipping normal faults and the role of the weak lower crust. *Gondwana Res.* 53, 20–40.
- Connolly, J.A.D., Petrini, K., 2002. An automated strategy for calculation of phase diagram sections and retrieval of rock properties as a function of physical conditions. *J. Metamorph. Geol.* 20, 697–708.
- Corfu, F., Hanchar, J.M., Hoskin, P.W.O., Kinny, P., 2003. Atlas of zircon textures. In: Hanchar, J.M., Hoskin, P.W.O. (Eds.), *Zircon. Reviews in Mineralogy and Geochemistry*, vol. 53. Mineralogical Society of America, Washington DC, pp. 27–62.
- Corti, G., Maestrelli, D., Sani, F., 2022. Large-to local-scale control of pre-existing structures on continental rifting: examples from the Main Ethiopian Rift, East Africa. *Front. Earth Sci.* 10. <https://doi.org/10.3389/feart.2022.808503>.
- Cuevas, J., Navarro-Vilá, F., Tubía, J., 2001. Evolución estructural poliorogénica del complejo Maláguense (Cordilleras Béticas). *Bol. Geol. Min.* 112, 47–58.
- Cuevas, J., Esteban, J.J., Tubía, J.M., 2006. Tectonic implications of the granite dyke swarm in the Ronda peridotites (Betic Cordilleras, Southern Spain). *J. Geol. Soc. London* 163, 631–640.
- Davies, G.R., Nixon, P.H., Pearson, D.G., Obata, M., 1993. Tectonic implications of graphitized diamonds from the Ronda, peridotite massif, southern Spain. *Geology* 21, 471–474.
- Díaz-Alvarado, J., Castro, A., Fernández, C., Moreno-Ventas, I., 2011. Assessing bulk assimilation in cordierite-bearing granitoids from the Central System Batholith, Spain; experimental, geochemical and geochronological constraints. *J. Petrol.* 52, 223–256.
- Díaz-Alvarado, J., Pedrera, A., Azor, A., García-Senz, J., Díaz de Neira, J.A., Rodríguez-Fernández, L.R., 2021. Submarine basaltic magmatism in the Subbetic Basin (southern Spain): Insights into melt-weakening processes during Mesozoic continental rifting. *Lithosphere* 5505884. <https://doi.org/10.2113/2021/5505884>.
- Esteban, J.J., Cuevas, J., Tubía, J.M., Liati, A., Seward, D., Gebauer, D., 2007. Timing and origin of zircon-bearing chlorite schists in the Ronda peridotites (Betic Cordilleras, Southern Spain). *Lithos* 99, 121–135.
- Esteban, J.J., Cuevas, J., Vegas, N., Tubía, J.M., 2008. Deformation and kinematics in a melt-bearing shear zone from the Western Betic Cordilleras (Southern Spain). *J. Struct. Geol.* 30, 380–393.
- Esteban, J.J., Cuevas, J., Tubía, J.M., Sergeev, S., Larionov, A., 2011a. A revised Aquitanian age for the emplacement of the Ronda peridotites (Betic Cordilleras, southern Spain). *Geol. Mag.* 148, 183–187.
- Esteban, J.J., Tubía, J.M., Cuevas, J., Vegas, N., Sergeev, S., Larionov, A., 2011b. Peri-Gondwanan provenance of pre-Triassic metamorphic sequences in the western Alpujarride nappes (Betic Cordillera, southern Spain). *Gondwana Res.* 20, 443–449.
- Esteban, J.J., Cuevas, J., Tubía, J.M., 2022. Peri-Gondwanan Provenance and Geodynamic Evolution of The Guadaiza Nappe (Alpujarride Complex, Betic Cordilleras, Spain): Insights on The Paleotethyan Paleogeography. *Minerals* 12, 325.
- Fallot, P., 1948. Les Cordillères Bétiques. *Etud. Geol.* IV, 83–172.
- Forshaw, J.B., Pattison, D.R.M., 2022. Major element geochemistry of pelites. *Geology* 51 (1), 39–43.
- Frasca, G., Gueydan, F., Poujol, M., Brun, J.-P., Parat, F., Monié, P., Pichat, A., Mazier, S., 2017. Fast switch from extensional exhumation to thrusting of the Ronda Peridotites (South Spain). *Terra Nova* 29, 117–126.
- Frost, R.B., Barnes, C.G., Collins, W.J., Arculus, R.J., Ellis, D.J., Frost, C.D., 2001. A geochemical classification for granitic rocks. *J. Petrol.* 42 (11), 2033–2048.
- Garrido, C.J., Bodinier, J.L., 1999. Diversity of mafic rocks in the Ronda peridotite: Evidence for pervasive melt-rock reaction during heating of subcontinental lithosphere by upwelling asthenosphere. *J. Petrol.* 40, 729–754.
- Garrido, C.J., Gueydan, F., Booth-Rea, G., Précigout, J., Hidas, K., Padrón-Navarta, J.A., Marchesi, C., 2011. Garnet lherzolite and garnet-spinel mylonite in the Ronda peridotite: Vestiges of Oligocene backarc mantle lithospheric extension in the western Mediterranean. *Geology* 39, 927–930. <https://doi.org/10.1130/G31760.1>.
- Gill, R.C.O., Aparicio, A., El Azzouzi, M., Hernandez, J., Thirlwall, M.F., Bourgeois, J., Marriner, G.F., 2004. Depleted arc volcanism in the Alboran Sea and shoshonitic volcanism in Morocco: geochemical and isotopic constraints on Neogene tectonic processes. *Lithos* 78, 363–388.
- Gómez-Pugnaire, M.T., Galindo-Zaldívar, J., Rubatto, D., Gonzalez-Lodeiro, F., Sanchez-Vizcaino, V.L., Jabaloy, A., 2004. A reinterpretation of the Nevado-Filabride and Alpujarride Complexes (Betic Cordillera): field, petrography and U-Pb ages from orthogneisses (western Sierra Nevada, S Spain). *Schweiz. Mineral. Petro. Mitt.* 84, 303–322.
- Gómez-Romeu, J., Masini, E., Tugend, J., Ducoux, M., Kuszniir, N., 2019. Role of rift structural inheritance in orogeny highlighted by the Western Pyrenees case-study. *Tectonophysics* 766, 131–150.
- González-Jiménez, J.M., Marchesi, C., Griffin, W.L., Gervilla, F., Belousova, E.A., Garrido, C.J., Romero, R., Talavera, C., Leisen, M., O'Reilly, S.Y., Barra, F., Martin, L., 2017. Zircon recycling and crystallization during formation of chromite- and Ni-arsenide ores in the subcontinental lithospheric mantle (Serranía de Ronda, Spain). *Ore Geol. Rev.* 90, 193–209. <https://doi.org/10.1016/j.oregeorev.2017.02.012>.
- Gueydan, F., Mazzotti, S., Tiberi, C., Cavin, R., Villaseñor, A., 2019. Western Mediterranean subcontinental mantle emplacement by continental margin obduction. *Tectonics* 38, 2142–2157.
- Herron, M., 1988. Geochemical Classification of Terrigenous Sands and Shales from Core or Log Data. *J. Sediment. Res.* 58 (5), 820–829.
- Hidas, K., Booth-Rea, G., Garrido, C.J., Martínez-Martínez, J.M., Padrón-Navarta, J.A., Konc, Z., Giacomia, F., Frets, E., Marchesi, C., 2013a. Back-arc basin inversion and subcontinental mantle emplacement in the crust: kilometre-scale folding and shearing at the base of the proto-Alborán lithospheric mantle (Betic Cordillera, southern Spain). *J. Geol. Soc. London* 170, 47–55.
- Hidas, K., Garrido, C.J., Tommasi, A., Padrón-Navarta, J.A., Thielmann, M., Konc, Z., Frets, E., Marchesi, C., 2013b. Strain localization in pyroxenite by reaction-enhanced softening in the shallow subcontinental lithospheric mantle. *J. Petrol.* 54, 1997–2031.
- Hidas, K., Tommasi, A., Garrido, C.J., Padrón-Navarta, J.A., Mainprice, D., Vauchez, A., Barou, F., Marchesi, C., 2016. Fluid-assisted strain localization in the shallow subcontinental lithospheric mantle. *Lithos* 262, 636–650.
- Hoepfner, R., Hoppe, P., Mollat, H., Muchow, S., Dürr, S., Kockel, F., 1963. Über den westlichen abschnitt der Betschen Kordilleren und seine beziehungen zum gesamtrogen. *Geol. Rundsch.* 53, 269–296.
- Hoepfner, R., Hoppe, P., Dürr, S., Mollat, H., 1964. Ein querschnitt durch die Betschen Kordilleren bei Ronda (SW Spanien). *Geol. Mijnb.* 43, 282–298.
- Holland, T.J.B., Powell, R., 1998. An internally consistent thermodynamic data set for phases of petrological interest. *J. Metamorph. Geol.* 16, 309–343.

- Holland, T.J.B., Powell, R., 2011. An improved and extended internally consistent thermodynamic dataset for phases of petrological interest, involving a new equation of state for solids. *J. Metamorph. Geol.* 29, 333–383.
- Homonnay, E., Corsini, M., Lardeaux, J.-M., Romagny, A., Münch, P., Bosch, D., Cenki-Tok, B., Ouazzani-Touhami, M., 2018. Miocene crustal extension following thrust tectonic in the Lower Sebitides units (internal Rif, Ceuta Peninsula, Spain): Implication for the geodynamic evolution of the Alboran domain. *Tectonophysics* 722, 507–535.
- Huismans, R.S., Beaumont, C., 2011. Depth-dependent extension, two-stage breakup and cratonic underplating at rifted margins. *Nature* 473, 74–78.
- Huismans, R.S., Beaumont, C., 2014. Rifted continental margins: The case for depth-dependent extension. *Earth Planet. Sci. Lett.* 407, 148–162. <https://doi.org/10.1016/j.epsl.2014.09.032>.
- Jabaloy-Sánchez, A., Padrón-Navarta, J.A., Gómez-Pugnaire, M.T., López Sánchez-Vizcaino, V., Garrido, C.J., 2019. Alpine orogeny: deformation and structure in the southern Iberian margin (Betics s.l.). In: Quesada, C., Oliveira, J. (Eds.), *The Geology of Iberia: A Geodynamic Approach*. Regional Geology Reviews. Springer. doi: 10.1007/978-3-030-11295-0_10.
- Jammes, S., Manatschal, G., Lavier, L., Masini, E., 2009. Tectonosedimentary evolution related to extreme crustal thinning ahead of a propagating ocean: Example of the western Pyrenees. *Tectonics* 28, TC4012. <https://doi.org/10.1029/2008TC002406>.
- Johanesen, K., Platt, J.P., Kaplan, M.S., Ianno, A.J., 2014. A revised thermal history of the Ronda peridotite, S. Spain: New evidence for excision during exhumation. *Earth Planet. Sci. Lett.* 393, 187–199.
- Lagabrielle, Y., Labaume, P., de Saint Blanquat, M., 2010. Mantle exhumation, crustal denudation, and gravity tectonics during Cretaceous rifting in the Pyrenean realm (SW Europe): Insights from the geological setting of the Iherzolite bodies. *Tectonics* 29, TC4012.
- Lenoir, X., Garrido, C.J., Bodinier, J.L., Dautria, J.M., Gervilla, F., 2001. The recrystallization front of the Ronda peridotite: Evidence for melting and thermal erosion of subcontinental lithospheric mantle beneath the Alboran basin. *J. Petrol.* 42, 141–158.
- Loneragan, L., White, N., 1997. Origin of the Betic-Rif mountain belt. *Tectonics* 16, 504–522.
- Loomis, T.P., 1972. Contact metamorphism of pelitic rock by the Ronda ultramafic intrusion, southern Spain. *Geol. Soc. Am. Bull.* 83, 2449–2474.
- Loomis, T.P., 1975. Tertiary mantle diapirism, orogeny, and plate tectonics east of the Strait of Gibraltar. *Am. J. Sci.* 275, 1–30.
- Ludwig, K.R., 2003. Mathematical-Statistical Treatment of Data and Errors for 230Th/U Geochronology. *Rev. Mineral. Geochem.* 52, 631–656.
- Lundeen, M.T., 1978. Emplacement of Ronda Peridotite, Sierra Bermeja. *Spain. Geol. Soc. Am. Bull.* 89, 172–180.
- Manatschal, G., 2004. New models for evolution of magma-poor rifted margins based on a review of data and concepts from West Iberia and the Alps. *Int. J. Earth Sci.* 93, 432–466. <https://doi.org/10.1007/s00531-004-0394-7>.
- Manatschal, G., Lavier, L.L., Chenin, P., 2015. The role of inheritance in structuring hyperextended rift systems: Some considerations based on observations and numerical modeling. *Gondwana Res.* 27, 140–164. <https://doi.org/10.1016/j.gr.2014.08.006>.
- Martín-Algarra, A., Vera, J.A., 2004. Evolución de Cordillera Bética. in: Vera, J.A. (Ed.), *Geología de España SGE-IGME*, Madrid, pp. 437–444.
- Martín-Algarra, A., Mazzoli, S., Perrone, V., Rodríguez-Cañero, R., 2009. Variscan tectonics in the Malaguide Complex (Betic Cordillera, Southern Spain): Stratigraphic and structural Alpine versus Pre-Alpine constraints from the Ardales Area (Province of Malaga). *II. Structure. J. Geol.* 117, 263–284.
- Massonne, H.-J., 2014. Wealth of P-T-t information in medium-high grade metapelites: Example from the Jubrique Unit of the Betic Cordillera, S Spain. *Lithos* 208–209, 137–157.
- Mazzoli, S., Martín-Algarra, A., 2011. Deformation partitioning during transpressional emplacement of a ‘mantle extrusion wedge’: the Ronda peridotites, western Betic Cordillera, Spain. *J. Geol. Soc. London* 168, 373–382.
- Michard, A., Goffe, B., Bouybaouene, M.L., Saddiqi, O., 1997. Late Hercynian-Mesozoic thinning in the Alboran domain: metamorphic data from the northern Rif, Morocco. *Terra Nova* 9, 171–174.
- Miller, C.F., McDowell, S.M., Mapes, R.W., 2003. Hot and cold granites? Implications of zircon saturation temperatures and preservation of inheritance. *Geology* 31, 529–532.
- Mohn, G., Manatschal, G., Beltrando, M., Haupt, I., 2014. The role of rift-inherited hyper-extension in Alpine-type orogens. *Terra Nova* 26, 347–353.
- Montel, J.M., Kornprobst, J., Vielzeuf, D., 2000. Preservation of old U-Th-Pb ages in shielded monazite: example from the Beni Bousera Hercynian kinzigites (Morocco). *J. Metamorph. Geol.* 18, 335–342.
- Montero, P., Bea, F., Corretgé, L.G., Floor, P., Whitehouse, M.J., 2008. U-Pb ion microprobe dating and Sr and Nd isotope geology of the Galí/Oeiro Igneous complex: a model for the peraluminous/peralkaline duality of the Cambro-Ordovician magmatism of Iberia. *Lithos* 107, 227–238.
- Morley, C.K., 1993. Discussion of origins of hinterland basins to the Rif-Betic Cordillera and Carpathians. *Tectonophysics* 226, 359–376.
- Muñoz, M., 1991. Significado de los cuerpos de leucogranitos y de los “gneises cordieríticos con litoclastos” asociados en la Unidad de Guadaíza (Alpujarrides occidentales, Béticas). *Geogaceta* 9, 10–13.
- Müntener, O., Hermann, J., Trommsdorff, V., 2000. Cooling history and exhumation of lower crustal granulite and Upper Mantle (Malenco, Eastern Central Alps). *J. Petrol.* 41 (2), 175–200.
- Navarro-Vilá, F., Tubía, J.M., 1983. Attempt at a new differentiation of the Alpujarride nappes in the western part of the Betic Cordilleras (Andalusia, Spain). *C. r. Acad. Sci. Ser. II* 296, 111–114.
- O'Connor, J.T., 1965. A classification of quartz rich igneous rock based on feldspar ratios. *US Geological Survey* 525B, 79–84.
- Obata, M., 1980. The Ronda peridotite - garnet-Iherzolite, spinel-Iherzolite, and plagioclase-Iherzolite facies and the P-T trajectories of a high temperature mantle intrusion. *J. Petrol.* 21, 533–572.
- Obata, M., 1994. Material transfer and local equilibria in a zoned kelyphite from a garnet pyroxenite, Ronda. *Spain. J. Petrol.* 35, 271–287.
- Patiño-Douce, A.E., 1995. Experimental generation of hybrid silicic melts by reaction of high Al basalt with metamorphic rocks. *J. Geophys. Res.* 100 (B8), 15623–15639.
- Pedreira, A., Ruiz-Constán, A., Galindo-Zaldívar, J., Chalouan, A., Sanz de Galdeano, C., Marín-Lechado, C., Ruano, P., Benmakhlof, M., Akil, M., López-Garrido, A.C., Chabli, A., Ahmamu, M., González-Castillo, L., 2011. Is there an active subduction beneath the Gibraltar orogenic arc? Constraints from Pliocene to present-day stress field. *J. Geodyn.* 52 (2), 83–96. <https://doi.org/10.1016/j.jog.2010.12.003>.
- Pedreira, A., Galindo-Zaldívar, J., Acosta-Vigil, A., Azor, A., González-Menéndez, L., Rodríguez-Fernández, L.R., Ruiz-Constán, A., 2016. Serpentinization-driven extension in the Ronda mantle slab (Betic Cordillera, S. Spain). *Gondwana Res.* 37, 205–215. <https://doi.org/10.1016/j.gr.2016.05.008>.
- Pedreira, A., García-Senz, J., Ayala, C., Ruiz-Constán, A., Rodríguez-Fernández, L.R., Robador, A., González-Menéndez, L., 2017. Reconstruction of the exhumed mantle across the North-Iberian Margin by crustal-scale 3D gravity inversion and geological cross-section. *Tectonics* 36, 3155–3177.
- Pedreira, A., Ruiz-Constán, A., García-Senz, J., Azor, A., Marín-Lechado, C., Ayala, C., Díaz de Neira, J.A., Rodríguez-Fernández, L.R., 2020. Evolution of the South-Iberian paleomargin: From hyperextension to continental subduction. *J. Struct. Geol.* 138, 104122.
- Pedreira, A., García-Senz, J., Peropadre, C., Robador, A., López-Mir, B., Díaz-Alvarado, J., Rodríguez-Fernández, L.R., 2021. The Getxo crustal-scale cross-section: testing tectonic models in the Bay of Biscay-Pyrenean rift system. *Earth Sci. Rev.* 212, 103429.
- Pedreira, A., García-Senz, J., Pueyo, E.L., López-Mir, B., Silva-Casal, R., Díaz-Alvarado, J., 2023. Inhomogeneous rift inversion and the evolution of the Pyrenees. *Earth Sci. Rev.* 245, 104555. <https://doi.org/10.1016/j.earscirev.2023.104555>.
- Pereira, M.F., Castro, A., Chichorro, M., Fernández, C., Díaz-Alvarado, J., Martí, J., Rodríguez, C., 2014. Chronological link between deep-seated processes in magma chambers and eruptions: Permo-Carboniferous magmatism in the core of Pangaea (Southern Pyrenees). *Gondwana Res.* 25, 290–308.
- Pérez-Gussinyé, M., 2013. A tectonic model for hyperextension at magma-poor rifted margins: An example from the West Iberia-Newfoundland conjugate margins. *Geol. Soc. Spec. Publ.* 369, 403–427. <https://doi.org/10.1144/SP369>.
- Peron-Pinvidic, G., Manatschal, G., ‘IMAGINING RIFTING’ workshop participants, 2019. Rifted margins: state of the art and future challenges. *Front. Earth Sci.* 7. <https://doi.org/10.3389/feart.2019.00218>.
- Peron-Pinvidic, G., Fourel, L., Buitier, S.J.H., 2022. The influence of orogenic collision inheritance on rifted margin architecture: Insights from comparing numerical experiments to the Mid-Norwegian margin. *Tectonophysics* 828, 229273.
- Peron-Pinvidic, G., Osmundsen, P.T., 2020. From orogeny to rifting: insights from the Norwegian ‘reactivation phase’. *Sci. Rep.* 10, 14860.
- Piles Mateo, E., Chamón Cobos, C., Estévez González, C., 1978. Mapa y memoria explicativa de la hoja 1065 (Marbella) del Mapa Geológico Nacional a escala 1: 50.000. Instituto Geológico y Minero de España, Madrid, España, 65.
- Platt, J.P., Argles, T.W., Carter, A., Kelley, S.P., Whitehouse, M.J., Loneragan, L., 2003a. Exhumation of the Ronda peridotite and its crustal envelope: Constraints from thermal modelling of a P-T-time array. *J. Geol. Soc., London* 160 (5), 655–676. <https://doi.org/10.1144/0016-764902-108>.
- Platt, J.P., Whitehouse, M.J., Kelley, S.P., Carter, A., Hollick, L., 2003b. Simultaneous extensional exhumation across the Alboran Basin: Implications for the causes of late orogenic extension. *Geology* 31, 251–254.
- Platt, J.P., Behr, W.M., Johanesen, K., Williams, J.R., 2013. The Betic-Rif arc and its orogenic hinterland: a review. *Annu. Rev. Earth Planet. Sci.* 41, 313–357.
- Powell, R., Holland, T.J.B., Worley, B., 1998. Calculating phase diagrams involving solid solutions via non-linear equations, with examples using THERMOCALC. *J. Metamorph. Geol.* 16, 577–588.
- Préçigout, J., Gueydan, F., Gapais, D., Garrido, C.J., Essaifi, A., 2007. Strain localization in the subcontinental mantle - a ductile alternative to the brittle mantle. *Tectonophysics* 445, 318–336.
- Préçigout, J., Gueydan, F., Garrido, C.J., Cogne, N., Booth-Rea, G., 2013. Deformation and exhumation of the Ronda peridotite (Spain). *Tectonics* 32, 1011–1025.
- Préçigout, J., Prigent, C., Palasse, L., Pochon, A., 2017. Water pumping in mantle shear zones. *Nat. Commun.* 8, 15736.
- Remaïdi, M., 1993. Étude pétrologique et géochimique d’une association péridotites refractaires-pyroxénites dans le Massif de Ronda (Espagne). Université de Montpellier II, France, p. 389. Ph.D. thesis.
- Rossetti, F., Theye, T., Lucci, F., Bouybaouene, M.L., Dini, A., Gerdes, A., Phillips, D., Cozzupoli, D., 2010. Timing and modes of granite magmatism in the core of the Alboran Domain, Rif chain, northern Morocco: Implications for the Alpine evolution of the western Mediterranean. *Tectonics* 29, TC2017.
- Royden, L.H., 1993. Evolution of retreating subduction boundaries formed during continental collision. *Tectonics* 12, 629–638.

- Ruiz Cruz, M.D., Sanz de Galdeano, C., 2014. Garnet variety and zircon ages in UHP meta-sedimentary rocks from the Jubrique zone (Alpujarride Complex, Betic Cordillera, Spain): evidence for a pre-Alpine emplacement of the Ronda peridotite. *Int. Geol. Rev.* 56 (7), 845–868. <https://doi.org/10.1080/00206814.2014.904759>.
- Ruiz-Constán, A., Galindo-Zaldívar, J., Pedrera, A., Célérier, B., Marín-Lechado, C., 2011. Stress distribution at the transition from subduction to continental collision (northwestern and central Betic Cordillera). *Geochem. Geophys. Geosyst.* 12, Q12002.
- Sánchez-Gómez, M., García Dueñas, V., Muñoz, M., 1995. Structural relationships between the Bermeja peridotites and the underlying Alpujarride units (Benahavis, Ronda, Spain). *Cr. Acad. Sci. II A* 321, 885–892.
- Sánchez-Navas, A., García-Casco, A., Mazzoli, S., Martín-Algarra, A., 2017. Polymetamorphism in the Alpujarride complex, betic cordillera, south Spain. *J. Geol.* 125 (6), 637–657. <https://doi.org/10.1086/693862>.
- Sánchez-Navas, A., Martín-Algarra, A., Blanco-Quintero, I., García-Casco, A., 2024. Pre-Alpine prograde evolution of the Upper Alpujarride (Betic-Rif belt) reveals a Paleotethys-related collision. *Int. Geol. Rev.* 66, 405–438. <https://doi.org/10.1080/00206814.2023.2246546>.
- Sánchez-Rodríguez, L., 1998. Pre-Alpine and Alpine evolution of the Ronda Ultramafic Complex and its country-rocks (Betic chain, southern Spain): U-Pb SHRIMP zircon and fission-track dating. Switzerland, ETH Zürich, Zürich, p. 170.
- Sánchez-Rodríguez, L., Gebauer, D., 2000. Mesozoic formation of pyroxenites and gabbros in the Ronda area (southern Spain), followed by Early Miocene subduction metamorphism and emplacement into the middle crust: U-Pb sensitive high-resolution ion microprobe dating of zircon. *Tectonophysics* 316, 19–44.
- Sanz de Galdeano, C., 2017. Implication of the geology of the Guadaiza and Verde valleys (Malaga Province, Betic Cordillera) on the position of the Ronda peridotites and the structure of the Alpujarride Complex. *Bol. Geol. Min.* 128, 989–1006.
- Sanz de Galdeano, C., 2023. Discussion on the differentiation of tectonic units in the Alpujarride Complex (Betic Cordillera). *Estud. Geol.* 79, e151.
- Sanz de Galdeano, C., López Garrido, Á.C., 2016. Geometry of the contact of the peridotites of Sierra Alpujata with the Sierra Blanca succession (Alpujarride Complex, Betic Internal Zone). *Geogaceta* 60, 7–10.
- Sanz de Galdeano, C., Ruiz Cruz, M.D., 2016. Formaciones del Paleozoico superior al Triásico depositadas discordantes sobre las peridotitas de Ronda: Evidencia de su emplazamiento cortical durante el Herciniano. *Estud. Geol.* 72, e043.
- Sánchez-Gómez, M., Balanya, J.C., García-Duenas, V., Azanon, J.M., 2002. Intracrustal tectonic evolution of large lithosphere mantle slabs in the western end of the Mediterranean orogen (Gibraltar arc). in: Rosenbaum, G., Lister, G.S. (Eds.), *Reconstruction of the evolution of the Alpine-Himalayan orogen*. Journal of the Virtual Explorer, pp. 23–34.
- Sosson, M., Morillon, A.C., Bourgeois, J., Féraud, G., Poupeau, G., Saint-Marc, P., 1998. Late exhumation stages of the Alpujarride complex, western Betic Cordilleras, Spain; new thermochronological and structural data on Los Reales and Ojen nappes. *Tectonophysics* 285, 253–273. [https://doi.org/10.1016/S0040-1951\(97\)00274-6](https://doi.org/10.1016/S0040-1951(97)00274-6).
- Soto, J.J., Platt, J.P., 1999. Petrological and structural evolution of high-grade metamorphic rocks from the floor of the Alboran Sea basin, western Mediterranean. *J. Petrol.* 40 (1), 21–60.
- Soustelle, V., Tommasi, A., Bodinier, J.L., Garrido, C.J., Vauchez, A., 2009. Deformation and reactive melt transport in the mantle lithosphere above a large-scale partial melting domain: the Ronda Peridotite Massif, southern Spain. *J. Petrol.* 50, 1235–1266.
- Steiger, R.H., Jäger, E., 1977. Subcommission on geochronology: convention on the use of decay constants in geo- and cosmochronology. *Earth Planet. Sci. Lett.* 36, 359–362.
- Sylvester, P.J., 1998. Post-collisional strongly peraluminous granites. *Lithos* 45, 29–44.
- Tajčmanová, L., Connolly, J.A.D., Cesare, B., 2009. A thermodynamic model for titanium and ferric iron solution in biotite. *J. Metamorph. Geol.* 27, 153–164.
- Theunissen, T., Huismans, R.S., 2022. Mantle exhumation at magma-poor rifted margins controlled by frictional shear zones. *Nat. Commun.* 13 (1), 1634. <https://doi.org/10.1038/s41467-022-29058-1>.
- Thiebot, E., Gutscher, M.-A., 2006. The Gibraltar Arc seismogenic zone (part 1): Constraints on a shallow east dipping fault plane source for the 1755 Lisbon earthquake provided by seismic data, gravity and thermal modeling. *Tectonophysics* 426, 135–152.
- Torres-Roldán, R.L., 1981. Plurifacial metamorphic evolution of the Sierra Bermeja peridotite aureole (Southern Spain). *Estud. Geol.* 37, 115–133.
- Torres-Roldán, R.L., 1983. Fractionated melting of metapelite and further crystal-melt equilibria—The example of the Blanca unit migmatite complex, north of Estepona (Southern Spain). *Tectonophysics* 96, 95–123.
- Tubía, J.M., 1985. Sucesiones metamórficas asociadas a rocas ultramáficas en los Alpujarrides Occidentales (Cordilleras Béticas, Málaga). University of País Vasco, p. 263. Ph.D. thesis.
- Tubía, J.M., 1988. Estructura de los Alpujarrides occidentales: cinemática y condiciones de emplazamiento de las peridotitas de Ronda. Parte II: Metamorfismo. *Bol. Geol. Min.* 99, 28–43.
- Tubía, J.M., Cuevas, J., 1986. High-temperature emplacement of the Los Reales peridotite nappe (Betic Cordillera, Spain). *J. Struct. Geol.* 8, 473–482.
- Tubía, J.M., Navarro-Vilá, F., Cuevas, J., 1993. The Maláguide-Los Reales nappe - An example of crustal thinning related to the emplacement of the Ronda peridotites (Betic Cordillera). *Phys. Earth Planet. Inter.* 78, 343–354.
- Tubía, J.M., Cuevas, J., Ibarguchi, J.G., 1997. Sequential development of the metamorphic aureole beneath the Ronda peridotites and its bearing on the tectonic evolution of the Betic Cordillera. *Tectonophysics* 279, 227–252. [https://doi.org/10.1016/S0040-1951\(97\)00124-8](https://doi.org/10.1016/S0040-1951(97)00124-8).
- Tubía, J.M., Cuevas, J., Esteban, J.J., Gil Ibarguchi, J.I., 2009. Remnants of a Mesozoic rift in a subducted terrane of the Alpujarride Complex (Betic Cordilleras, southern Spain). *J. Geol.* 117, 71–87.
- Tubía, J.M., Cuevas, J., Esteban, J.J., 2013. Localization of deformation and kinematic shift during the hot emplacement of the Ronda peridotites (Betic Cordilleras, southern Spain). *J. Struct. Geol.* 50, 148–160.
- Tugend, J., Manatschal, G., Kuszniir, N.J., Masini, E., Mohn, G., Thonon, I., 2014. Formation and deformation of hyperextended rift systems: insights from rift domain mapping in the Bay of Biscay-Pyrenees. *Tectonics* 33, 1239–1276.
- Van der Wal, D., Bodinier, J.L., 1996. Origin of the recrystallisation front in the Ronda peridotite by km-scale pervasive porous melt flow. *Contrib. Mineral. Petrol.* 122, 387–405.
- Van der Wal, D., Vissers, R.L.M., 1993. Uplift and emplacement of upper-mantle rocks in the Western Mediterranean. *Geology* 21, 1119–1122.
- Van der Wal, D., Vissers, R.L.M., 1996. Structural Petrology of the Ronda Peridotite, SW Spain: Deformation History. *J. Petrol.* 37, 23–43.
- Vauchez, A., Garrido, C.J., 2001. Seismic properties of an asthenospherized lithospheric mantle: constraints from lattice preferred orientations in peridotite from the Ronda massif. *Earth Planet. Sci. Lett.* 192, 235–249.
- Vauchez, A., Barrool, G., Tommasi, A., 1997. Why do continents break-up parallel to ancient orogenic belts? *Terra Nova* 9, 62–66.
- Vera, J.A., Ancochea, A., Calvo Sorando, J.P., Barnolas Cortinas, A., Bea Carredo, F., 2004. Geología de España. España, Instituto Geológico y Minero de España, Madrid, p. 884.
- Vergés, J., Fernández, M., 2012. Tethys-Atlantic interaction along the Iberia-Africa plate boundary: The Betic-Rif orogenic system. *Tectonophysics* 579, 144–172.
- Villaseca, C., Barbero, L., Herreros, V., 1998. A re-examination of the topology of peraluminous granite types in intracontinental orogenic belts. *Trans. Roy. Soc. Edinb. Earth Sci.* 89, 113–119.
- Watson, E.B., Harrison, T.M., 1983. Zircon saturation revisited - temperature and composition effects in a variety of crustal magma types. *Earth Planet. Sci. Lett.* 64, 295–304.
- White, R.W., Powell, R., Holland, T.J.B., Johnson, T.E., Green, E.C.R., 2014a. New mineral activity-composition relations for thermodynamic calculations in metapelitic systems. *J. Metamorph. Geol.* 31, 261–286.
- White, R.W., Powell, R., Johnson, T.E., 2014b. The effect of Mn on mineral stability in metapelites revisited; new a-x relations for manganese-bearing minerals. *J. Metamorph. Geol.* 32, 809–828.
- Whitehouse, M.J., Platt, J.P., 2003. Dating high-grade metamorphism—constraints from rare-earth elements in zircon and garnet. *Contrib. Mineral. Petrol.* 145, 61–74.
- Whitmarsh, R.B., Manatschal, G., Minshull, T.A., 2001. Evolution of magma-poor continental margins from rifting to seafloor spreading. *Nature* 413 (6852), 150–154.
- Whitney, D.L., Evans, B.W., 2010. Abbreviations for rock-forming minerals. *Am. Mineral.* 95, 185–187.
- Williams, I.S., 1998. U-Th-Pb geochronology by ion microprobe. In: McKibben, M.A., Shanks, W.C., III, Ridley, W.I. (Eds.), *Applications of Microanalytical Techniques to Understanding Mineralizing Processes*. Rev. Ec. Geol., pp. 1–35.
- Williams, I.S., Claesson, S., 1987. Isotopic evidence for the Precambrian provenance and Caledonian metamorphism of high grade paragneisses from the Seve Nappes, Scandinavian Caledonides, II ion microprobe zircon U-Th-Pb. *Contrib. Mineral. Petrol.* 97, 205–217.
- Zheng, Y.F., Chen, R.X., 2021. Extreme metamorphism and metamorphic facies series at convergent plate boundaries: Implications for supercontinent dynamics. *Geosphere* 17, 1647–1685.
- Zheng, Y.F., Gao, P., 2021. The production of granitic magmas through crustal anatexis at convergent plate boundaries. *Lithos* 402–403, 106232.
- Zheng, Y.F., Chen, Y.X., Chen, R.X., Dai, L.Q., 2022. Tectonic evolution of convergent plate margins and its geological effects. *Sci. China Earth Sci.* 65, 1247–1276.